

TRENDS IN FORMING AND WELDING OF STAINLESS STEELS

H. Hänninen, J. Romu

Helsinki University of Technology, Finland

Abstract

Various new forming techniques (hydroforming, superplastic forming and hot metal gas forming) have become an alternative to various stamping processes. The technologies are still rather new and there is not yet enough information available to assist the product design and manufacturing. Welding of stainless steels is still often based on the conventional welding techniques, but recently high energy density laser and electron beam welding techniques as well as solid-state friction stir welding have become the new alternative techniques. This paper reviews the new trends in forming technologies and the emerging new welding techniques for stainless steel products.

Introduction

Manufacturing of products from stainless steels meets increasing demands for efficiency in terms of cost savings and increased productivity. This has led to the development of new forming methods, which can overcome the disadvantages of traditional forming and joining manufacturing methods. In all these methods the aim is to manufacture products which have complex shapes formed in one forming operation reducing, thus, the amount of working steps needed in conventional manufacturing based on welding of stampings, etc. Additionally, these methods offer a possibility to obtain improved material properties and microstructures of the manufactured products.

Welding technology of stainless steels is still often based on the conventional welding techniques, but recently high energy density laser and electron beam welding techniques have been used increasingly for the welding of the austenitic and ferritic stainless steels in specialized applications. These techniques offer advantages over conventional welding techniques, such as low heat input, small HAZ, low distortion and residual stresses, and high welding speed. Friction stir welding is an emerging solid-state technique where a rotating tool with pin and shoulder is inserted in the material to be joined and traversed along the line of joint. The heating is localized, and is generated by friction between the tool and the work piece, with additional adiabatic heating from metal deformation. When considering the operational performance of stainless steel weldments the most important things are corrosion resistance, weld mechanical properties and the integrity of the welded joint. These properties are mainly influenced by the metallurgical processes occurring during welding or heat treatment of the welded component, i.e., solidification of the weld metal, and recrystallization as well as the precipitation phenomena. These phenomena have to be well understood to obtain maximum corrosion resistance and mechanical properties for the stainless steel weldments. Other problems with welded stainless steel structures in addition to possibility of defects (porosity, cracks, slag inclusions etc.) are residual stresses and distortion. Due to local heating

during welding, complex thermal stresses and residual strain (due to shrinkage) distributions occur after welding, which are especially deleterious in the thick-wall components of the energy industry.

Forming

Hydroforming

Hydroforming is a process where tubular or sheet preforms are placed in a die at room temperature and after closing of the die with high locking forces internal water or water-oil mixtures are pressurized up to 6000 bar and the preform obtains the shape of the die, Figure 1. Main applications of hydroformed parts are in the automotive and aircraft industries. The advantages of hydroforming as compared with conventional manufacturing methods via stamping and welding include: 1) possibility to manufacture more complex parts in one operation as compared with multiple working steps in conventional manufacturing, 2) weight reduction through more efficient section design and tailoring of the wall thickness in different parts of the product, 3) increased strength and stiffness of the manufactured products, 4) lower tooling costs as a result of lower amount of parts, 5) less secondary operations needed, 6) dimensional tolerances are tight and springback low and 7) reduced amount of scrap. The disadvantages of the process in comparison to conventional stamping and welding are: 1) cycle times are relatively slow, 2) equipment is expensive and 3) new welding techniques are needed. In general, one disadvantage of hydroformed parts as well as for the conventionally manufactured parts is the residual stresses of the parts, which adversely affect their dimensional accuracy. The total cycle times of hydroformed parts can be reduced by integrating secondary operations (piercing and bending, etc.) to the hydroforming process. Typically, pre-bent or pre-deep-drawn preforms are needed for hydroformed parts, which increase the total cycle time and costs of the process [1, 2].

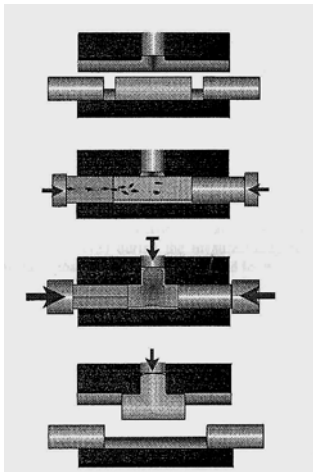


Figure 1. Principle of hydroforming process [1].

Materials selection for hydroformed parts depends on the required final properties of the part, forming process as well as material deformation capabilities, availability and cost. Generally, materials selection is a compromise between obtainable properties, formability and cost of the material. Stainless steels have good formability, which allows to design more complex parts that would need several manufacturing steps with conventional stamping and welding. Additionally, the good formability of stainless steels and possibility to manufacture more consolidated products make them a potential material to replace other materials, such as carbon steels, and offer possibilities to

weight reduction of the components. Selection of stainless steels depends on the application and environments where the hydroformed parts are to be used. Strength, corrosion resistance, etc. of the component can be adjusted by choosing the suitable stainless steel grade. The most commonly used stainless steel is EN 1.4301 due to the combination of formability, corrosion resistance, strength and cost [1, 2].

Hydroforming technology development is nowadays influenced by light-weight products, increased functional integration of the manufactured components and the increased experience in using hydroformed parts. Efforts in development work in hydroforming are concentrating on reducing the cycle times and costs of the whole process chain. Especially, one of the limiting factors of the production rate of hydroforming is bending/pre-forming operations needed before the actual forming. It has led to utilization of several bending/pre-form units to supply the preforms to the hydroforming press. Alternatively, hydroforming presses have been built, which can form several parts in one cycle. Computer simulation of the manufactured parts and the hydroforming process has greatly improved the profitability of the process. Efforts have been lately concentrated to obtaining better modelling of formability of materials and components. This has required determination of Forming Limit Diagrams of several mainly tubular materials using internal pressure with and without axial feeding. Additionally, development work has been focusing on helping to choose the right type of lubricant allowing to reduce friction between the formed part and the die, thus, improving the efficiency of the process [1, 2].

Superplastic forming

Superplastic forming is based on forming of components at elevated temperatures with gas pressure into dies. Superplasticity allows unusually large elongations (> 500% without necking) under low stresses if temperature and strain rate are chosen correctly. The benefits of superplastic forming include possibility to manufacture complex structures, avoidance of spring back and residual stresses, suitability for short production runs, possibility to reduce or even eliminate working operations as well as cost and weight savings. The drawback of superplastic forming is the still relatively long forming cycle (from few minutes to 20 – 30 min), which limits the production quantities/year. Superplastic forming has traditionally been used in aerospace applications and the materials used have been for superplastic forming especially developed tailor-made materials (mainly titanium and aluminium alloys) with special alloying and/or complex thermomechanical treatments in order to obtain desired microstructure suitable for forming. However, recently less expensive commercial grade materials have been studied in order to make them amenable for superplastic forming. Demands for cost savings have awakened improvements to improve the effectiveness of the whole process as well as interest in the possibility to superplastically form austenitic stainless steels, since they are amenable for superplastic forming with relatively simple thermomechanical treatment and are also less costly materials. Additionally, they offer a possibility to lower the forming temperature (650 – 800°C vs. 900 – 1050°C for duplex stainless steel grades). However, until now, the forming pressures needed are clearly higher (peak flow stresses 100 – 200 MPa) and the elongations obtained (400 - 600%) are lower than those for duplex stainless steel grades (elongations > 1000% and peak flow stresses 10 – 50 MPa). Strain rates obtained during forming are in the range of 10^{-4} – 10^{-3} s⁻¹ for austenitic grades and 10^{-4} – 10^{-2} s⁻¹ for the duplex grades, Figure 2. The trend in duplex stainless steel has been focused on developing new “lean” duplex stainless steels, which from a superplastic forming point of view luckily have a wider forming temperature range and reduced risk for intermetallic phase precipitation, Figure 2. A

superplastically formed name plate and tubular shape made from EN 1.4162 duplex stainless steel are shown in Figure 3 [3-12].

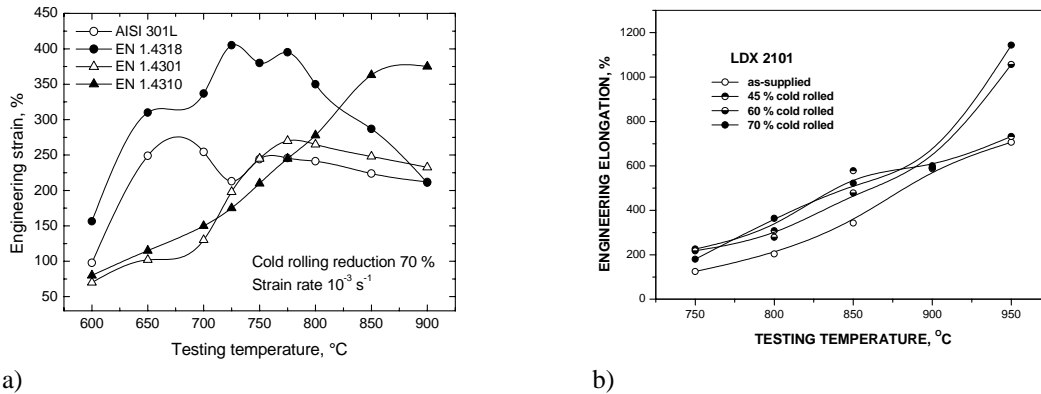


Figure 2. Temperature dependencies of engineering strain in hot tensile tests for cold rolled (reduction 70%) austenitic stainless steels a) and as-supplied and cold-rolled (reduction 45 – 70%) EN 1.4162 (LDX 2101) duplex stainless steel b). The nominal initial strain rate in all tests was 10^{-3} s^{-1} [6, 10].

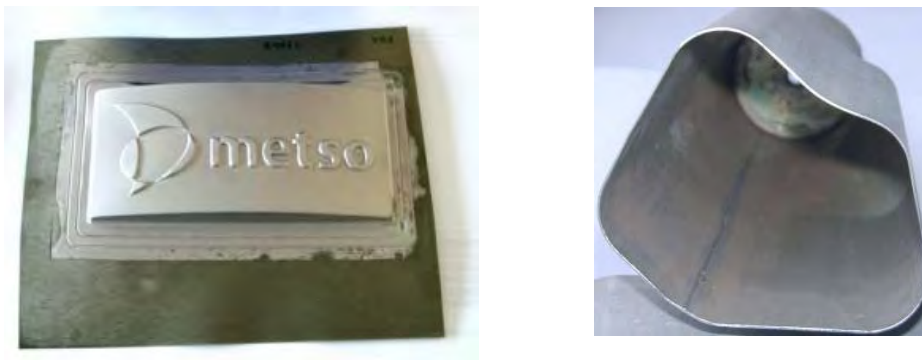


Figure 3. Products made with superplastic forming at FormTech GmbH from EN 1.4162 duplex stainless steel.

Hot metal gas forming

Hot metal gas forming is a process that combines *in-situ* induction heating of a tubular or flat sheet workpiece to elevated forming temperatures in a ceramic die, and shaping the work piece in a die cavity using gas pressure. The forming includes also quenching of the formed part in a separate die. Hot metal gas forming has been developed from superplastic forming process and hot blow forming process used in the plastics industry in high-volume production. When compared with superplastic forming the strain rates and forming pressures are higher, whereas the obtainable amount of deformation is lower for hot metal gas forming. Production rates are, thus, higher in hot metal gas forming (few seconds) as compared with those for superplastic forming (from few minutes up to 20 – 30 min/part). On the other hand, superplastic forming allows manufacturing of more complex shapes with optimal die filling, whereas hot metal gas forming of stainless steels has been suffering from full die filling within reasonable forming time. This has been mainly overcome by using axial feeding of the workpiece during forming [13-16].

Hot gas metal forming was developed by automobile manufacturing industry to compete with hydroforming. Majority of the products made have been formed from tubular preforms. The production rates of hot gas metal forming are in the same range as those for hydroforming. When

compared with hydroforming hot gas metal forming has some advantages. Production costs can be lowered, since the forming machines are cheaper (appr. 50% cheaper than hydroforming presses) due to the low pressures needed (2 – 5% of those for hydroforming presses). The ceramic dies used are cheaper and faster to manufacture as compared with the tool-steel dies used in hydroforming. The total manufacturing cycle times are generally in the order of 10 – 15 s depending on the material and part geometry to be made, which is reported to result in 2 – 3 times higher production rates than in hydroforming. One benefit is also the possibility to use more common materials in forming as compared with those used in hydroforming. Alltogether it has been stated that hot gas metal forming can be 35 – 40% less expensive than hydroforming when cost savings obtained from equipment, tooling material and productivity issues area taken into account. Additionally, hot gas metal formed parts can have significantly improved material characteristics including microstructure, mechanical properties, freedom of residual stresses and consequently the dimensional precision is improved reducing the need for secondary finishing operations. Limitations of hot gas metal forming as compared with hydroforming include the relatively short die life of the ceramic dies with embedded induction coils, longer die change-over times due to the hot dies and need for certain secondary operations like creation of holes into the formed products. Also, pre-bending or pre-deep drawing operations are needed sometimes in order to obtain the desired final shape of the product, which is an additional manufacturing step [13-16].

Hot metal gas forming of stainless steels has been concentrating to ferritic stainless steel EN 1.4512. Austenitic grades (EN 1.4301) have also been preliminarily tested but research was not continued due to the poorer formability as compared with the ferritic grades. Testing included free bulge tests and forming into a die of tube preforms with and without axial feeding. Heating of the tube preform was performed with Joule effect using electrical jaws. In the free bulge tests of the ferritic stainless steel EN 1.4512 55% diameter expansion was obtained at 960°C with a gas pressure of 14.75 bar in few seconds, Figure 4. With axial feeding during deformation the tube diameter expansion could be increased to 140%. In the case of forming of the tube preform in a cylindrical die problems were observed in obtaining sufficient filling of the die (95% filling) and local thinning of the tube without axial feeding. These problems could be overcome with axial feeding [17, 18].

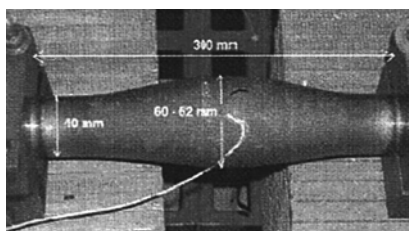


Figure 4. Free bulge test performed with hot metal gas forming of EN 1.4512 ferritic stainless steel [17].

Welding

High energy density laser and electron beam welding

Laser welding is an attractive process for joining of thin materials with fast travel speed and fast cooling rates. Thus, autogeneous laser welds of austenitic and duplex stainless steels tend to result in high ferrite contents, which may be affected by suitable filler additions. For ferritic and ferritic-martensitic stainless steels usually beneficial properties are obtained by laser welding. High energy density electron beam welding is especially suitable for heavy-section austenitic and duplex

stainless steel materials (around 50 mm) in one or two passes. The cooling rates are high, which again results in highly ferritic weld especially in thinner sections.

Friction stir welding

Friction stir welding (FSW) of stainless steels has been an interest recently, since FSW is expected to result in the formation of fine grains, low distortion and no segregation in the welding of stainless steels, which are definite advantages as compared to the fusion welding processes. The microstructural evolution in austenitic steel FSW shows typical dynamic recrystallization and recovered microstructures in the weld [18]. Since FSW does not accompany melting and solidification the phase transformations are minimized, which is especially important for duplex stainless steels, when significant refining of the ferrite/austenite microstructure without change in the phase ratio takes place [19]. FSW method has also been applied for thin sheets of precipitation hardened martensitic stainless steel PH 15-7 successfully [20]. The major problem of FSW of stainless steels is, however, that special very expensive tool materials such as PCBN or tungsten-rhenium alloy, are needed.

Summary

Various new forming techniques (hydroforming, superplastic forming and hot metal gas forming) have become an alternative to various stamping processes. The technologies are still rather new and there is not yet enough information available to assist the product design and manufacturing. Welding of stainless steels is still often based on the conventional welding techniques, but recently high energy density laser and electron beam welding techniques as well as solid-state friction stir welding have become the new alternative techniques in specialized applications.

References

- [1] M. Ahmetoglu and T. Altan, "Tube Hydroforming; State-of-the-Art and Future Trends", *J. Mater. Proc. Tech.*, 98(2000), pp. 25-33.
- [2] M. Liewald and S. Wagner, "State-of-the-Art of Hydroforming Tubes and Sheets in Europe", *Proc. of the International Conference TUBEHYDRO2007*, June 4 – 5, Harbin, China, pp. 19-26.
- [3] K. Mineura and K. Tanaka, *Journal of Materials Science*, 24(1989), pp. 2967-2970.
- [4] Y. Maehara, *Transactions of the ISIJ International*, 27(1987), pp. 705-712.
- [5] S. Takaki and T. Suzuki, *Proceedings of the International Congress Stainless Steel '99, Science and Market*, 1999, Vol. 2, pp. 49-56.
- [6] J. Pimenoff, J. Romu, Y. Yagodzinsky and H. Hänninen, "Superplasticity and Superplastic Forming in Finland - Recent Advancements and Future Prospects". 2nd Joint European Meeting on Superplasticity and Superplastic Forming (Euro-SPF 02), 13-15 June, 2002, Bristol, Great Britain, 8 p.
- [7] J. Romu, Y. Yagodzinsky, W. Beck and H. Hänninen, "Manufacturing of Shaped Forms from Stainless Steels with Superplastic Forming". *Proc. of the 8th International Conference on Superplasticity in Advanced Materials*, 28 - 30 July, 2003, St. Catherine's College, Oxford, UK, pp. 159-164.
- [8] Y. Yagodzinsky et al., *Mat. Sci. Tech.*, 20(2004), pp. 925-929.
- [9] Y. Maehara, and Y. Ohmori, *Met. Trans.*, 18A(1987), pp. 663-672.
- [10] K. Osada, *Proc. Conf. Superplasticity and Superplastic Forming*, eds. Hamilton, C.H. and Paton, N.E., *The Minerals, Metals & Materials Society*, 1988, pp. 429-433.

- [11] J. Romu, Y. Yagodzinsky, W. Beck and H. Hänninen, Proc. Conf. EUROSPPF04, The Third European Conference on SuperPlastic Forming, July 7-9, 2004, Ecole des Mines d'Albi-Carmaux, France, pp. 45-50.
- [12] J. Romu, Y. Yagodzinsky., S. Papula, W. Beck and H. Hänninen, "Effect of Forming Temperature and Cooling Rate on Superplastic Formability and Corrosion Resistance of EN 1.4162 Duplex Stainless Steel". Proc. of the 4th European Conference on Superplastic Forming - Euro SPF'05, June 22-24, 2005, Manchester, UK, pp. 73-77
- [13] G. Pfaffmann, X. Wu and W. Dykstra, "Hot Metal Gas Forming of Auto Parts", Adv. Mater. & Proc., 157, February 2000, pp. H35 – H37.
- [14] B. Dykstra, "Hot Metal Gas Forming for Manufacturing Vehicle Structural Components", Metal Forming (USA), 35(9), 2001, pp. 50-52.
- [15] B. Gardner, "The Business Case for the Use of Hot Metal Gas Forming", Metal Forming (USA), 35(10), 2001, pp. 36 – 37.
- [16] J. Benedyk, "Hot Metal Gas Forming of Aluminum for Manufacturing Vehicle Structural Components", Light Metal Age, 61(11-12), 2003, pp. 16-19.
- [17] L. Vadillo et al., "Simulation and Experimental Results of the Hot Metal Gas Forming Technology for High Strength Steel and Stainless Steel Tubes Forming", Proc. of the Numiform '07, 9th International Conference on Numerical Methods in Industrial Forming Processes, American Institute of Physics, Vol. 908, 2007, pp. 1199 – 1204.
- [18] J. Zarazua, L. Vadillo, A. Mangas, M. Santos, M. Gutierrez, B. Gonzalez, C. Testani and S. Argentero, "Alternative Hydroforming Process for High Strength and Stainless Steel Tubing in the Automotive Industry", Proc. of the IDDRG 2007 International Conference, 21 – 23 May, 2007, Győr – Hungary, 2007, 8 p.
- [19] S. Park et al., Scripta Mat., 49(2003), pp. 1175-1180.
- [20] Y. Sato et al., Mat. Sci. Eng., A397(2005), pp. 376-384.
- [21] J. Mononen and H. Hänninen, "FSW of PH 15-7 Stainless Steel Sheet", Proc. of 6th International Conference on Friction Stir Welding, Saint-Sauveur, Canada, October 10-13, 2006, Paper 48.

SENSE AND SENSITIVITY OF THERMO-MECHANICAL FORMING SIMULATION OF METASTABLE AUSTENITIC STAINLESS STEELS

E. Ratte

ThyssenKrupp Nirosta GmbH, Germany

Abstract

Metastable austenitic stainless steels may transform to martensite during forming. The transformation itself is governed by the stacking fault energy (SFE) of the steel and indirectly affected by a variety of parameters. Material immanent parameters are the chemical composition and the austenite grain size whereas temperature and the occurring adiabatic heating affect the SFE during forming as well. Referring to experimental results, a critical martensite content is deviated in order to reduce the efforts in thermo-mechanical simulation. Different isothermal and non-isothermal models are discussed with regard to their applicability in forming or crash simulation.

Introduction

Austenitic steels are widely used in applications which require an extraordinary forming behaviour. This characteristic is determined by microstructural mechanisms that are governed by the low stacking fault energy (SFE) of these steels which is usually classified between 10 and 100 mJ/m² [1]. The low SFE leads to a change in the predominant hardening mechanism during forming. With decreasing SFE crystallographic gliding is more and more accompanied by twinning and finally by a strain induced martensite transformation.

As the formula for M_S or M_{D30} the SFE is a way to rank the stability of austenitic steels and as for these well-known equations the SFE was described empirically as a function of the chemical composition. In contrast to M_S and M_{D30} , the SFE is not a temperature. Nevertheless, it can be described as function of temperature. As an advantage the values for the SFE are a direct measure for the occurring forming mechanisms.

Influence of temperature

The most important factor on the SFE of a steel is the temperature. Rising temperatures lead to increasing values of the SFE which is reflected in decreasing amounts of martensite formed at elevated temperatures. Generally, the influence of the temperature on the SFE can be assumed to be linear. An increasing forming speed can be considered like an elevated temperature due to the adiabatic heating of the sample. Both result in an increase in SFE and therefore in a reduced martensite formation [3][4].

Influence of stress state

The second parameter which should be considered when modelling the martensite evolution is its dependency on the stress state during forming. The reason for the heterogeneous behaviour under different load conditions is the increase of volume which goes ahead with the martensitic

transformation. In a tensile stress state the formation of the martensite is favoured whereas under compression the increasing of volume is hindered. This will lead to higher amount of martensite in those forming operations where tensile load conditions appear and lower amounts of martensite in compression [2].

Experimental results

Martensite formation as function of temperature

Figure 1 shows the flow curves of steel 1.4376 measured at temperatures between -40 and 100°C. At temperatures between 40 and 100°C the curve has the general course like ferritic steels with decreasing strain hardening. The curves below 40°C indicate a plateau and two turning points which become much more pronounced with decreasing temperature. In this temperature range, high amounts of α' -martensite (above all α_γ) occur during straining which was already verified in former publications [3].

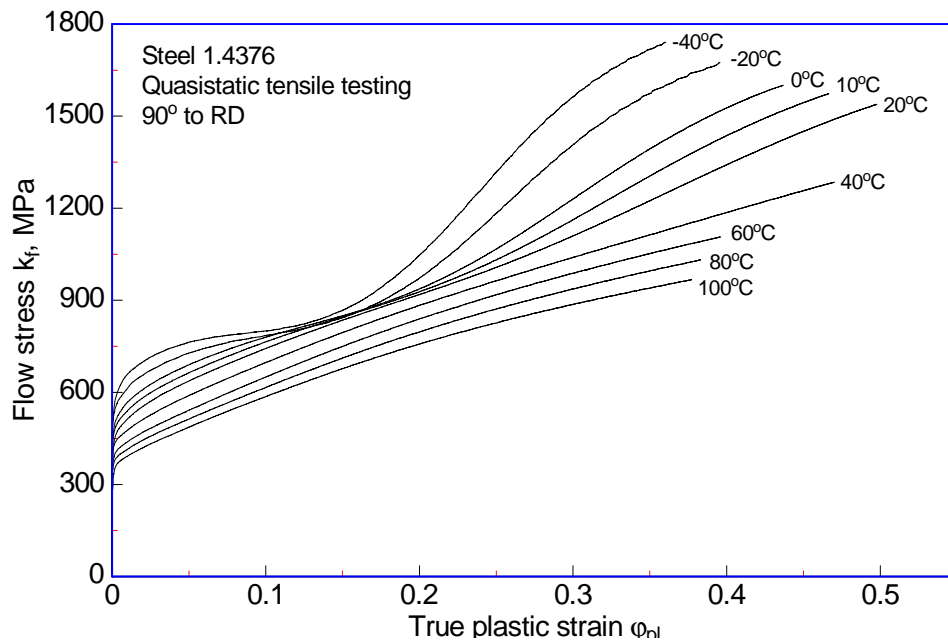


Figure 1. Flow curves of the austenitic stainless steel 1.4376 [4]

When comparing the maximum martensite fractions which were formed during the tensile test (Figure 2) it becomes obvious that at the temperature of the sudden change in the strain hardening behaviour the maximum martensite fraction, which was measured after testing, increases rapidly. A compilation of data from literature shows that the change in the strain hardening behaviour goes ahead with a martensite fraction of 20-30% [4][5][6].

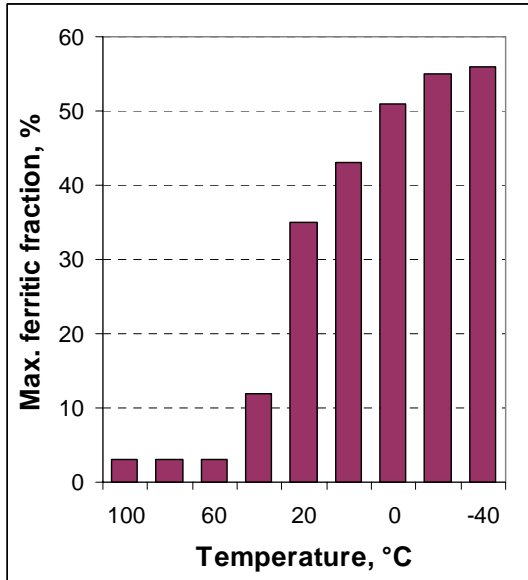


Figure 2. Maximum martensite fraction of steel 1.4376 after tensile testing [6]

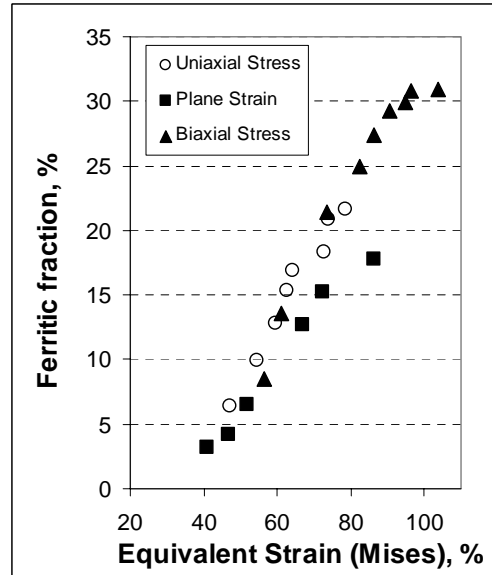


Figure 3. Maximum martensite fraction of steel 1.4301 in different stress states.

Martensite formation as function of stress state

As already mentioned the martensite formation strongly depends on the stress state present during forming. Figure 3 shall summarize the development of the martensite formation in different stress states. For the three stress states uniaxial tension, plane strain and biaxial tension, the martensite formation is given as a function of the equivalent strain according to von Mises. It becomes obvious, that the biaxial and uniaxial loads favour the martensite formation most. The curve which was measured under plane strain condition lies on a significantly lower level than those for uni- and biaxial stress. Nevertheless, figure 3 cannot present the influence of the stress state as a single parameter but is a mixed presentation of the influence of stress state and adiabatic heating due to the non-isothermal testing conditions.

Deviation of a critical martensite content

The stability of the austenitic stainless steels differs with their SFE energy which is governed by their chemical composition. At medium up to elevated temperatures austenitic steels use the same metalphysical mechanism during forming as ferritic steels do: gliding. Due to this, the strain hardening behaviour (e.g. the slope of the flow curve) is more or less comparable to those of common carbon steels albeit the austenitic steels show much higher elongation values.

When reaching a critical value between 20 and 25% of martensite the strain hardening behaviour changes completely. The percentage is comparable for all metastable austenitic steels. The reason for this critical martensite content lies in the possible distribution the martensite can show within the austenitic matrix, Figure 4.

If the second phase has a percentage of 25% it is theoretically still possible that this phase is distributed in islands. For the austenitic steels this would mean that there is still a non-interrupted austenitic matrix with relatively homogeneously distributed martensite islands. The work hardening is primarily determined by the work hardening of the austenitic phase. With increasing martensite content above 25% there will always be a network of martensite. The work hardening changes accordingly and will show a stronger increase due to the higher strength of the martensite.

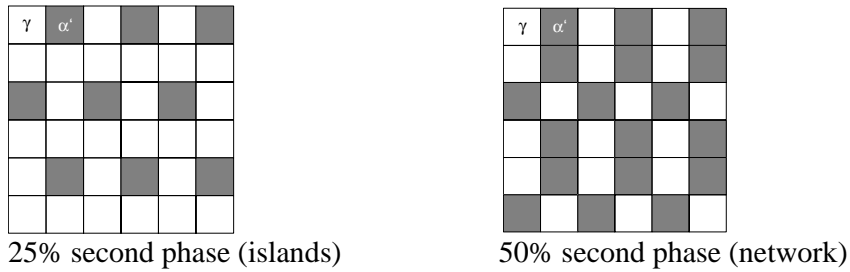


Figure 4. Comparison of possible distributions of two phases

In industrially produced steels it is possible that the distribution of martensite is not completely homogeneous. This is the reason why for several steels the change in the strain hardening behaviour can be observed at lower martensite contents (down to 20%). Generally, the martensite transformation has not to be taken into consideration in simulation if the fraction of martensite formed does not exceed 20%. This is valid for the martensite which is determined by the chemical composition of the steel but as well for the martensite which is formed under different temperatures and stress states. Processes with an extensive adiabatic heating (as Crash- or dynamic forming processes) do not necessarily have to take the martensitic transformation into account as long as the critical value of 20-25% is not exceeded.

Martensite evolution in simulation

Isothermal conditions

Olson and Cohen [7][8] described the transformation kinetics based on martensite nucleation at shear-band intersections in austenite.

$$V_{SB} = 1 - \exp(-\alpha \cdot \varepsilon)$$

V_{SB} – Number of shear bands
 α – Constant
 ε – Strain

The number of shear bands refers to a certain volume of austenite. The function includes a constant K which reflects the martensite geometry and an additional geometry exponent n. Finally a probability is calculated that two shearbands show an interface and martensite nucleation starts.

$$V_{M\%} = 1 - \exp(-\beta \cdot (1 - \exp(-\alpha \cdot \varepsilon))^n)$$

$V_{M\%}$ - Martensite volume
 β - Probability of martensite formation

One major problem of this model was the missing consideration of multi-axial load cases which exhibit a strong influence on the martensite formation. Hecker succeeded to model the influence of complex multi-axial stress states by implementing the equivalent strain according to von Mises which showed better results than the equivalent strain according to Tresca for steel 1.4301 [9]. Isothermal models are generally suitable in applications where the material does not change its temperature during deformation. This may be possible in several extremely slow forming operations or in those which offer an intensive temperature control as cooling or heating in combination with moderate forming speed.

Non-isothermal conditions

If the temperature changes during forming, e.g. as function of friction or adiabatic heating, non-isothermal models have to be chosen. The most important model which is nowadays available in several FE-codes is the Hänsel model. Hänsel reformulated the model of Ludwigson and Berger to be independent of strain in order to be able to simulate non-isothermal processes [10][11]. The martensite formation is given by

$$\frac{dV_m}{d\varepsilon} = \frac{B}{A} \cdot e^{\frac{Q}{T}} \cdot \left(\frac{1-V_m}{V_m} \right)^{\frac{1+B}{B}} \cdot V_m \cdot [0,5 \cdot (1 - \tanh(C + D \cdot T))] \quad \text{if } \varepsilon \geq E_0$$
$$\frac{dV_m}{d\varepsilon} = 0 \quad \text{if } \varepsilon < E_0$$

After integration the yield stress equation is given

$$\sigma_y = (B_{HS} - (B_{HS} - A_{HS}) \exp(-m(\varepsilon + \varepsilon_0)^n)) (K_1 + K_2 T) + \Delta H_{\gamma \rightarrow \alpha'} V_m$$

ε - effective plastic strain

V_m - martensite volume

T - temperature

σ_y - flow stress

A, B, C, D, p, Q, A_{HS} , B_{HS} , m, n, K_1 , K_2 , $\Delta H_{\gamma \rightarrow \alpha'}$, ε_0 - parameters

The authors refer to other and own works demonstrating the difficulty to simulate non-isothermal processes with an isothermal description. The reason for this is claimed to be the deformation and temperature history dependence of the martensite formation. In an industrial forming operation, the temperature is raising continuously during the process. An incremental, non-isothermal material model was formulated with respect to the forming history. The main disadvantage of the Hänsel-description is the large number of 14 (!) material parameters which has to be determined. This can be done by simple tensile tests equipped with an additional temperature- and martensite-measurement. Based on the model of Hänsel, a strongly simplified model was developed using neural networks by Heinemann [12]. With these models a thermo-mechanical modelling is possible and leads to improved results with respect to prediction of forces and stresses. Unfortunately, the direct consideration of the dependence on the stress state and strain rate is missing.

Conclusions for thermo-mechanical simulations

What do the previous chapters mean for sense and sensitivity of thermomechanical modelling?

- First, not all metastable austenitic steels which may show a martensitic transformation while forming have to be modelled thermo-mechanically. A thermo-mechanical simulation makes sense if the martensite fraction exceeds 20%. Lower contents allow a simplified modelling using the flow curve determined mainly by the austenite.
- The martensite fraction itself is governed by the SFE and therefore temperature-dependent. Non-constant forming temperature or an adiabatic heating result in a non-isothermal process which have to be considered with special thermo-mechanical models.
- In those cases, special attention has to be paid to the determination of correct material parameters. Nevertheless, the proposed model by Hänsel model with all its advantages is not sensitive to changes in stress state. Instable steels which show a marked martensite

formation in quasistatic forming may behave differently under multi-axial stresses due to the hindered or favoured martensite formation.

- Besides the conclusions above mentioned, the choice of the correct material description does not end at describing the martensite transformation properly. The use of suitable yield loci, friction values and failure criteria has a strong influence on the quality of simulation results and is a major topic of current research.

References

- [1] R.E. Schramm, R. Reed: "Stacking fault energies of seven commercial austenitic stainless steels", Metallurgical Transactions, 6A, 7, 1975, pp. 1345-1351
- [2] S.A. Kulin, M. Cohen, B.L. Averbach: Trans AIME, 1952, p.661
- [3] W. Bleck, G. Steinbeck: MP Materialprüfung, 43, 1-2, 2001 1-2, pp. 6-17
- [4] A. Frehn, E. Ratte, W. Bleck: Influence of temperature and strain rate on the mechanical properties and the formability of the austenitic stainless steel 1.4376 containing manganese and nitrogen, HNS 2004, Oostende,
- [5] E. Ratte: Wasserstoffinduzierte verzögerte Rissbildung austenitischer Stähle auf CrNi(Mn)- und Mn-Basis, Dr.-Ing. Diss, Aachen, 2007
- [6] A. Frehn: Einfluß von Umformtemperatur und -geschwindigkeit auf das Umformvermögen austenitischer nichtrostender Stähle, Dr.-Ing. Diss, Aachen, 2004
- [7] G.B. Olson, M. Cohen : Met trans A, 6A, 1975, p.791
- [8] G.B. Olson, M. Cohen: J. Less-Common Metals, 28, 1972, p. 107
- [9] S.S. Hecker u.a.: Metall. Trans. A, 13A, 1982, p. 619
- [10] A. Hänsel, P. Hora, J. Reissner: Model for the kinetics of strain-induced martensitic phase transformation at non isothermal conditions for the simulation of sheet metal forming processes with metastable austenitic steels, Sim. Mat. Proc: Theory, Methods and Appl, eds Hétnik & Baaijens, 1998 Balkema, Rotterdam, p. 373-378
- [11] A. Hänsel: Nichtisothermes Werkstoffmodell für die FE-Simulation von Blechumformprozessen mit metastabilen austenitischen CrNi-Stählen, PhD Thesis, Fortschr.-Ber. VDI Reihe 2 Nr. 491 Düsseldorf: VDI Verlag 1998
- [12] G. Heinemann: Virtual determination of forming limits of metastable austenitic stainless steels applied to sheet forming processes, Zürich, 2004

HOT METAL GAS FORMING FOR STAINLESS STEELS

*G. Martos¹, J. M^a. Castellanos¹, A. Bocardo¹, J. Contreras¹, D. Vallecillo¹, M. Guerra¹,
R. Sánchez¹, B. González², M. Gutiérrez², L. Vadillo², M. Santos², I. Zarazua²*

¹ACERINOX, S.A, Spain, ²FUNDACIÓN LABEIN, Spain

Abstract

The paper describes the work carried out to exam some aspects about the feasibility of applying a novel manufacturing process known as hot metal gas forming (HMGF) on austenitic and ferritic stainless steels. The work is part of the recently finished European RFS-CR-04034 project. Different experiments have been performed on 1.5 mm 2B sheets and 40x1.5 mm tubes of EN-1.4301 and EN-1.4512 steels. Process variables like heating rate, temperature and holding time were examined from tests conducted on a Gleeble 1500D machine as to their effects on the steels microstructure, thermal gradient built up on the specimen and the power angle of the electrical transformer. The effect of the heating process on the hot ductility (deformation stage of the HMGF process) was also determined through hot tensile tests. Subsequently, thickness and hardness scans and microstructural study of different prototype direct heating HMGF parts produced by LABEIN were carried out. In general, the free hot forming process gives, for the ferritic steel, more deformation and less symmetry compared to the room temperature hydraulic process. The process appears to be conveniently controlled when the deformation is done against a die and the axial feeding is properly set. The investigation has shown that the 12 Cr ferritic stainless studied is quite apt as to the HMGF process, and accordingly has been considered as a reference steel for new improvements of this technique.

Introduction

Important aspects of stainless steels sheet forming processes, which are usually carried out at room temperature, are the need of high or very high power machinery due to the high strength of these alloys and the continuous requirement of better formability and final properties. Accordingly, and in addition to materials optimization, searching for new processes which could lead to reduced investment and operation costs and enhanced fabrication and strength properties has always been a subject of interest by steel producers and manufacturers.

The hot metal gas forming (HMGF) is a process developed from the late 90s originally intending to achieve the above aims for metals like titanium and aluminium. It has hydroforming as its main reference technology. Basically, the HMGF is a two stage process in which the work piece is initially heated to deformation temperature, either by induction or direct heating, and then deformed by gas (usually air) pressure for which an air tighten system is to be provided. Flat and tubular products can be deformed by such HMGF process.

Once the basic HMGF concept has achieved a significant level of readiness for soft metals, a further challenge is to exam the potential of the process for high strength steels, including stainless grades. This is the main objective of the European RFS-CR-04034 project, from which the work described hereafter is extracted. The paper is focused on the feasibility of direct heating HMGF for common 12 Cr superferritic and 18-8 CrNi austenitic sheet and tubes through

laboratory tests in terms of post heating features and inherent ductility, and by characterizing prototype sheet and tube HMGF parts manufactured by LABEIN.

Materials and experimental

Stainless steel grades for the study were of the austenitic EN-1.4301 and ferritic EN-1.4512 types, in (2B, 1.5 mm) sheets and (2B, 40x1.5 mm) tubes manufactured from mill heats produced by ACERINOX which have the average compositions shown in Table 1. The tubes were manufactured by TIG welding (austenitic) and high frequency welding (ferritic).

Table 1. Chemical compositions of the sheet and tubes materials under study, in weight %. ASTM GS of sheets.

Steel grade	C	Si	Mn	Ni	Cr	S	N	Ti	GS
1.4301	0.049	0.26	1.76	8.16	18.3	0.005	0.0497	-	8.1
1.4512	0.010	0.46	0.23	0.16	11.7	0.001	0.0113	0.132	7.2

The work carried out to exam the feasibility of forming standard stainless steels by HMGF comprises three main areas, namely a) effect of the heating sequence on the steel grain size, transformer power angle and thermal gradient developed along the work piece; b) materials hot ductility; and c) features of prototype parts in terms of thinning, hardness and microstructure.

Test specimens for a) and b) tasks were directly prepared from delivery sheet samples, while both sheet and tube HMGF pieces for the c) study were produced by LABEIN using its own taylor-made devices, some of which are shown in Figure 1.



Figure 1. Experimental devices for the sheet (left) and tube (right) free expansion HMGF trials by LABEIN.

Effects of heating parameters

The main direct heating variables (heating rate, target temperature and holding time) were studied by ACERINOX on supply sheet samples through tests conducted on a Gleeble 1500D system, which heats the sample by Joule effect. The effects of these parameters were assessed as to the grain size which is present when the deformation process stage is to commence; the electrical transformer response (through the power angle parameter) to meet the heating programme; and the lengthwise thermal gradient which is built up on the test specimen between the grips of the heating device. The tests variables are shown in Table 2.

Table 2. Test parameters for the heating tests conducted on a Gleeble 1500D system.

Heating rate (°C/s)	Aim temperature (°C)	Holding time (s)
50	1000	0
100	1100	5
200	1200	10

Combining the above parameters has the referred effects which are shown in the figures that follow. Common Gleeble test features: 20 mm width flat specimens, copper jaws, K-type thermocouples (control in centered position, measuring 20 mm offset, 50 mm free span).

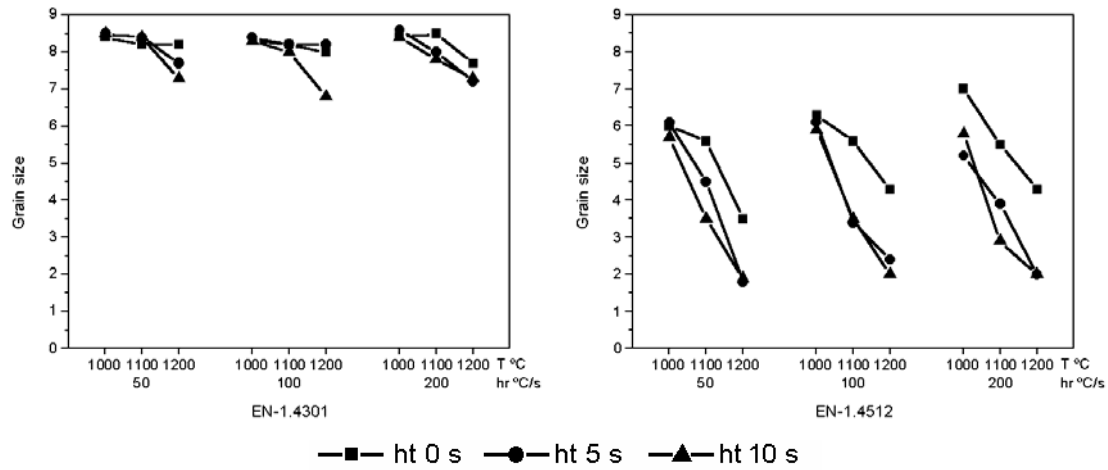


Figure 2. Gleeble heating tests: effect of test variables on the microstructure grain size.

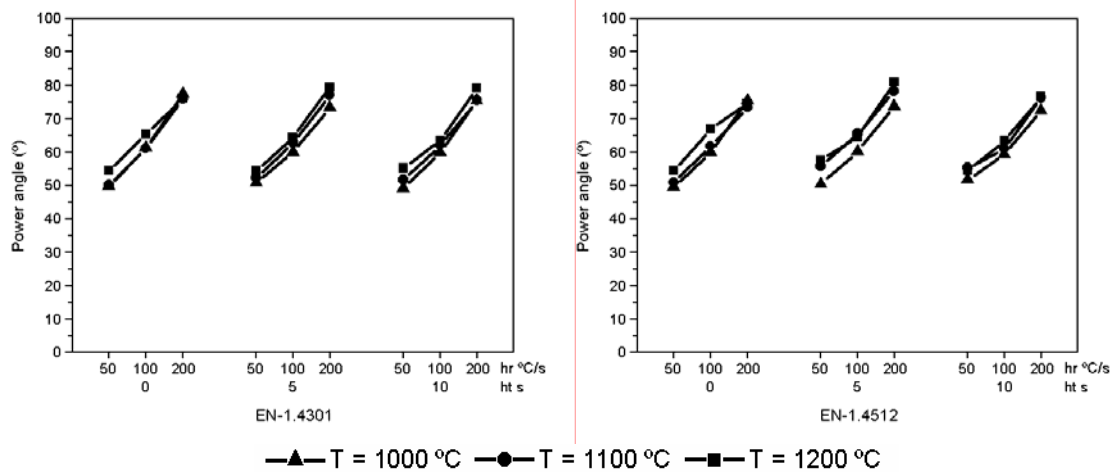


Figure 3. Gleeble heating tests: effect of test variables on the electrical transformer operation (power angle).

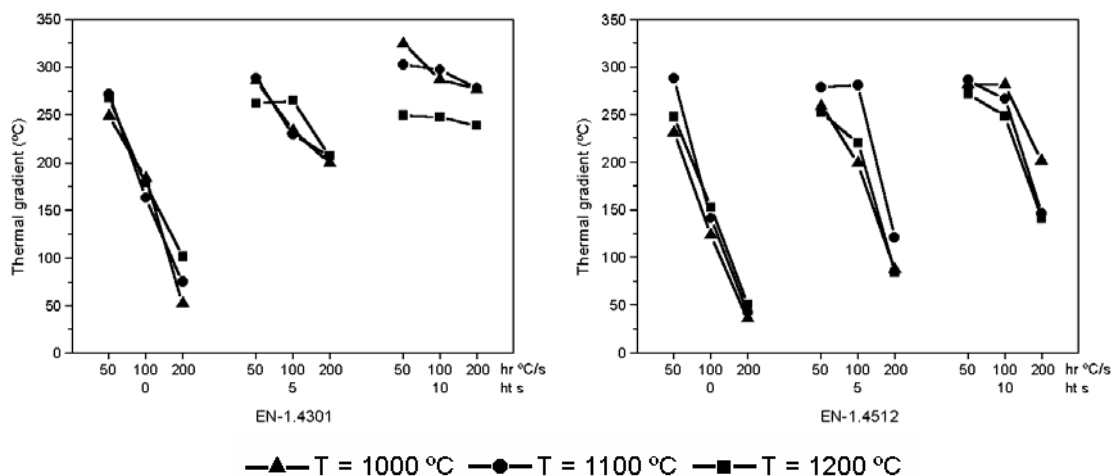


Figure 4. Gleeble heating tests: effect of test variables on the lengthwise thermal gradient measured between control and 20 mm offset thermocouples.

Hot ductility

In a high temperature deformation process, the features of the work piece, in terms of microstructure and temperature distribution at the point in which the deformation is to begin, are determined by the heating method (Joule effect in the case of the HMGF under study), the materials physical properties and the heating parameters. Counting on this, and bearing in mind that improving formability is expected to be an additional benefit of the HMGF process, the hot ductility of the stainless grades being studied was assessed by high temperature tensile tests conducted on the Gleeble system on samples heated under different heating conditions (shown in Table 3). Test arrangements were equal to those already used in the previous study on the effects of heating variables. The ductility was calculated from fracture reduction in width (in %).

Table 3. Test conditions for the Gleeble's hot ductility study.

Heating rate	°C/s	50, 100
Test temperature	°C	1000, 1100
Holding time	s	0, 5
Strain rate	1/s	0.1, 1.0

The test results are collected and shown in Figures 5 and 6.

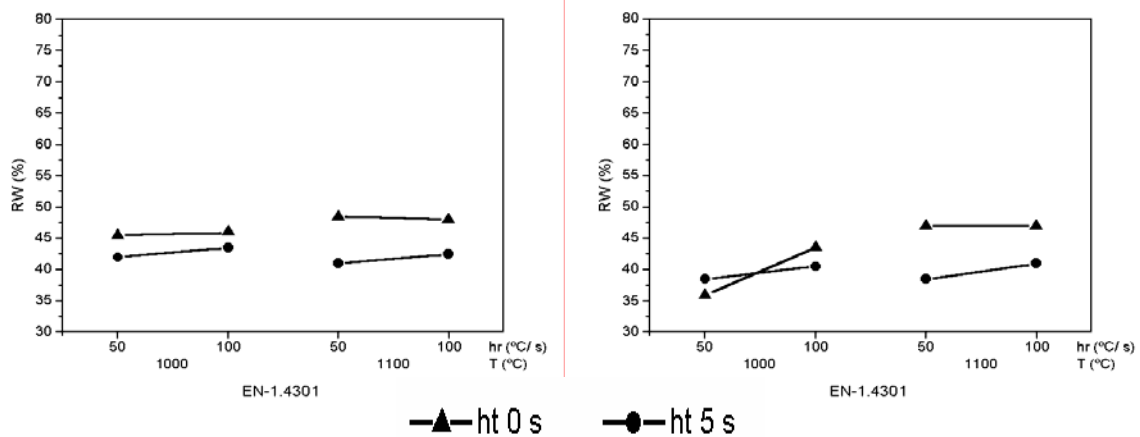


Figure 5. Gleeble hot ductility tests on the 1.4301 stainless grade: 0.1 1/s (left) and 1.0 1/s (right).

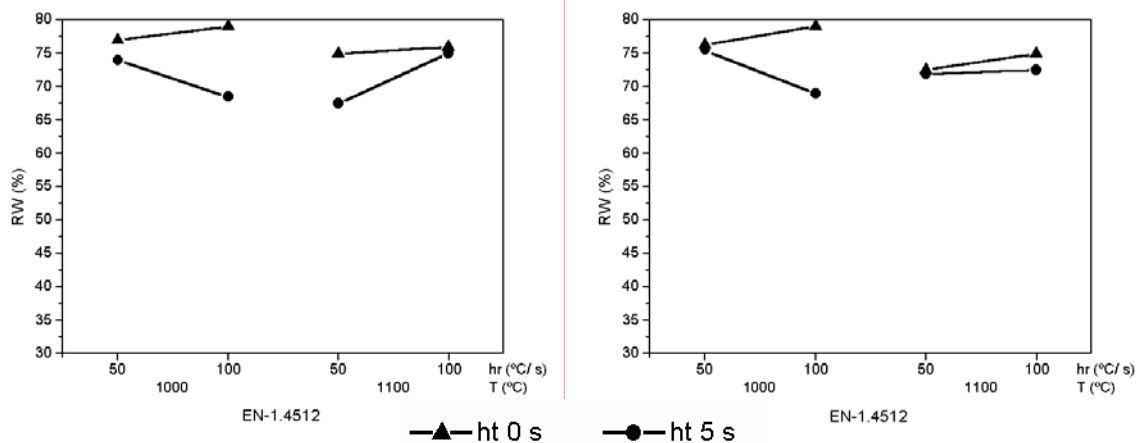


Figure 6. Gleeble hot ductility tests on the 1.4512 stainless grade: 0.1 1/s (left) and 1.0 1/s (right).

Characterization of prototype HMGF parts

The following experimental HMGF parts were produced and studied by LABEIN and ACERINOX, respectively. Circular hydraulic bulge ferritic sample is included as reference.

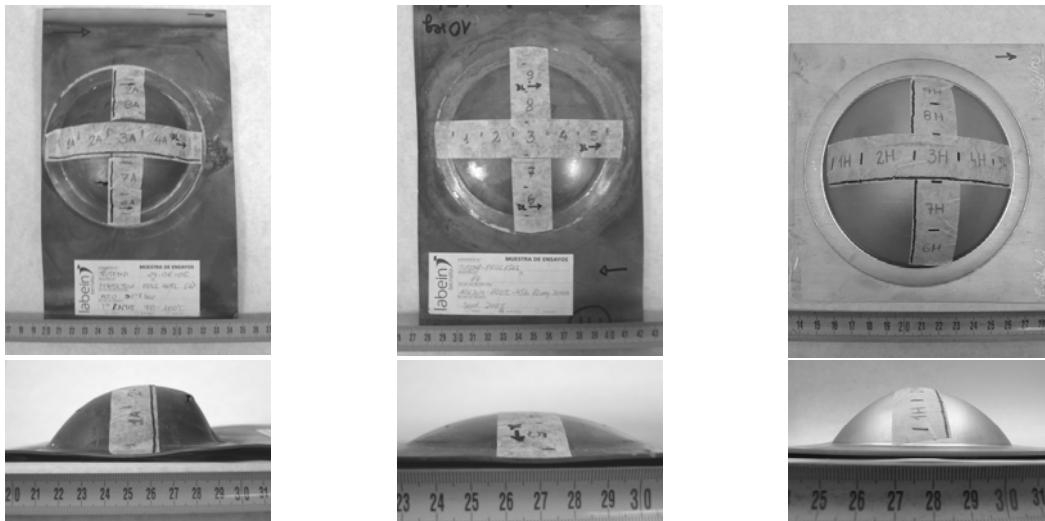


Figure 7. Sheet bulge tests: HMGF 950°C, 33 bar on ferritic (left), HMGF 1100°C, 45 bar, 10 s on austenitic (centre), and room temperature hydraulic test on ferritic (right).

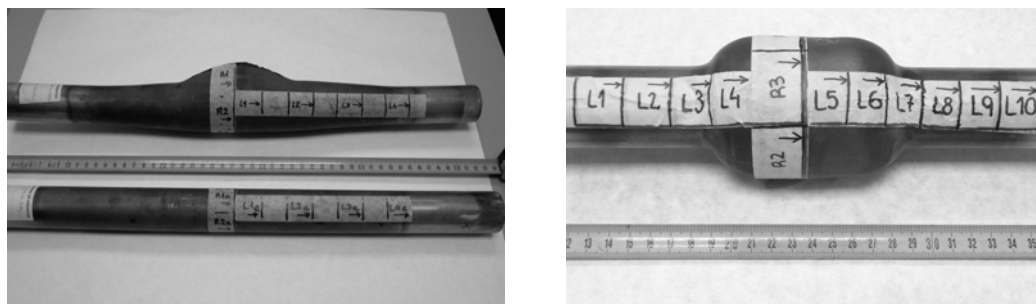


Figure 8. HMGF tube bulge tests: free expansion on ferritic at 1020°C, 10 bar, 10 s (left above) and on austenitic at 1100°C, 20 bar, 5 s (left below); and expansion against a die + axial feeding on ferritic at 950°C, 19 bar (right).

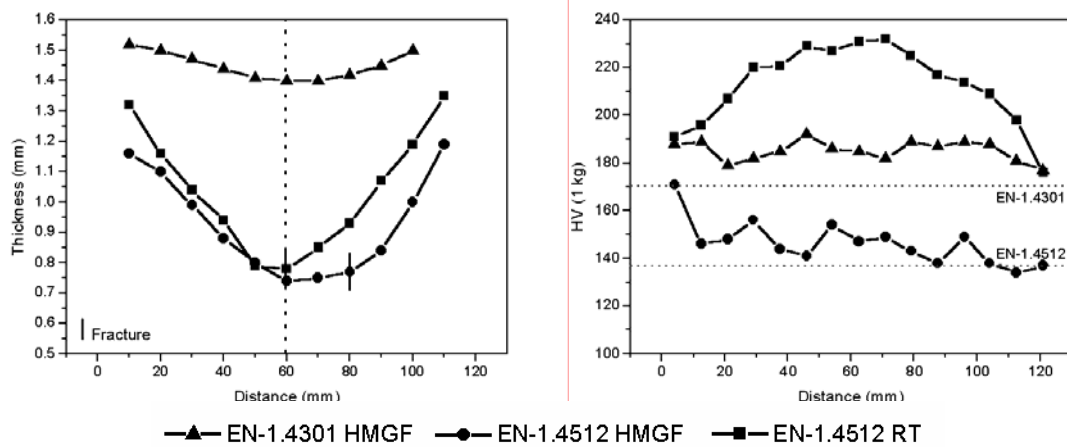


Figure 9. Thickness (left) and hardness (right) scans parallel to rolling direction on ferritic and austenitic free expansion sheet samples.

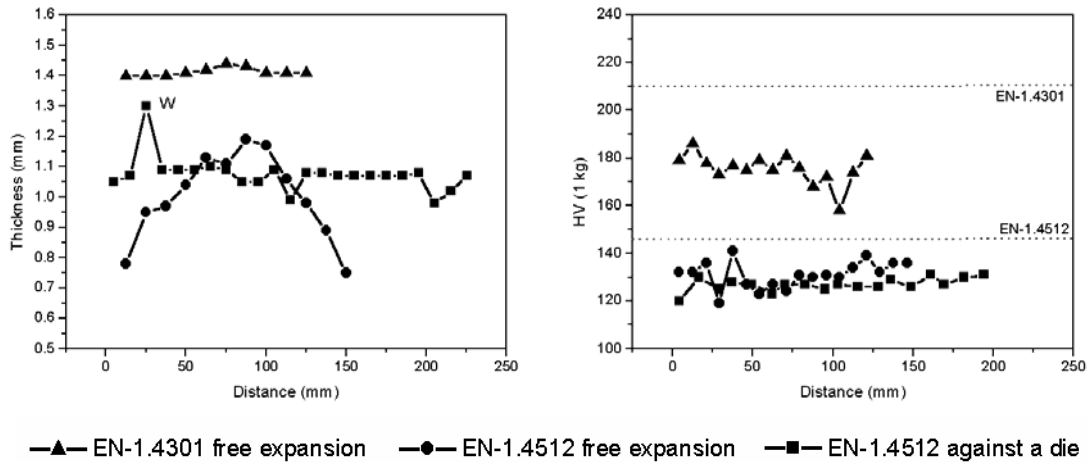


Figure 10. Thickness (left) and hardness (right) scans normal to rolling direction on ferritic and austenitic tubes.

Final comments and conclusions

The feasibility of the direct heating hot metal gas forming (HMGF) process for widely used stainless steels (12 Cr superferritic and 18-8 CrNi austenitic) has been examined in a twofold approach. First, through laboratory tests to address technology and metallurgy aspects of the direct heating process: microstructure and temperature profile after heating, and heating affected ductility. Secondly, by characterizing prototype sheet and tube HMGF parts made by LABEIN.

Compared to the austenitic, the ferritic stainless has been found to be more sensitive to the heating parameters, as derived from the verified straight effect of grain growth as a function of temperature and holding time. The power angle increase is directly related, to greater extent in the austenitic, to the heating rate and is not affected by the target temperature. The best hot ductility is achieved in the case of the fine grained ferritic material.

As to the prototype HMGF process itself, the study shows that the free expansion version of it tends to yield larger but more uneven deformation compared to the standard room temperature hydraulic counterpart process in the case of the ferritic sheet and tube. Comparatively, and for a given aim temperature, the stronger austenitic steel requests much higher air pressure. On the other hand, both reasonably uniform strain distribution and correct final features are achieved in the case of the ferritic steel tube produced by the constrained HMGF process.

Acknowledgement

The authors wish to recall that the above piece of work has been carried out with the financial support of the EC through the RFS-CR-04034 project, short named TUTEMP and jointly participated by LABEIN, IEHK, CSM, HGET, TNO and ACERINOX.

References

- [1] X. Wu, H.Hao, Y. Liu, F. Zhu, J. Jiang, R. Krishnamurthy, S. Wang, P.E. Smith, W.Bland, G.D. Pfaffmann, "Elevated temperature formability of some engineering metals for gas forming of automotive structures"
- [2] W. Dykstra, G.Pfaffmann, X. Wu, "Hot metal gas forming. The next generation process for manufacturing vehicle structural components"
- [3] RFS-CR-04034 project entitled "Plasticity at high temperature for tube forming applications in the automotive industry" – TUTEMP

LOCAL MARTENSITIC HIGH-STRENGTH STRUCTURE FIELDS – MATERIAL PROPERTIES OF METASTABLE AUSTENITIC STAINLESS STEEL

B.-A. Behrens, S. Hübner, K. Weilandt, K. Voges-Schwieger

Leibniz Universität Hannover, Germany

Abstract

The industrial application of stainless steels is of high importance, because of its high corrosion resistance and forming behaviour. However, there are also other extensive material properties considering metastable austenitic stainless steel. Actual industrial projects investigate the application of stainless steel as composition components in automotive engineering to realize a lightweight construction [1]. Due to the martensite evolution in deep drawing processes, the material affects an increase in strain-hardening. In the collaborative research centre 675 of DFG (German Research Foundation) - “Creation of high strength metallic structures and joints by setting up scaled local material properties”, this effect is being researched at the Institute of Metal Forming and Metal-Forming Machines (IFUM) of the Leibniz Universität Hannover. In the here described sub-project, the aim is the combination of different material properties for the generation of special load adapted components in forming operations e.g. crash relevant carrier systems. In this project, these parts are characterised by austenitic ductile regions and martensitic high-strength areas, generated in one deep drawing process of EN 1.4301 (AISI 304). To produce such stretched out areas, an applicable deep drawing tool is developed with defined additional forming elements. By these additional forming elements an increase in martensite concentration is effectuated.

To generate specific load adapted material properties, different investigations were conducted to research those attributes in crash- and Nakajima-tests. The material behaviour of local martensitic structure parts is analysed in a drop impact tester. A demonstrator part for carrier systems e.g. in automotive industry combines this austenitic and martensitic material behaviour in one part. A defined folding behaviour at crash impact can be determined for those structured parts due to the high energy absorption of martensite.

Moreover, Nakajima samples with martensitic structure fields as local strain-hardening are produced to get detailed information about the material behaviour of such combined properties. The determination of the Forming Curves of this modified material enables a first statement about the load-dependent application area regulated on the state of stress. In order to realize an applicable adaptation of material properties for the application area, it is very important to determine best stress and strain states to design components. The material characterisation of these combined properties in one material shows auspicious perspectives for forthcoming investigations to apply different attributes in parts made of one metastable stainless steel. Further investigations will consider more metastable steels to compare differences in respective material behaviour.

Introduction

The good forming and crash behaviour of metastable austenitic steels like the EN 1.4301 is well-known. To generate load-adapted components with locally different material properties, the strain-induced martensite transformation during deep drawing is utilised. Additional forming elements in a deep drawing tool effect an increase in strain-hardening due to martensite evolution. Martensite generation is a transformation from an austenitic ductile fcc-lattice into a high-strength α' -martensitic-lattice. In other cases, the austenite transforms into a non-stable hcp-lattice of the ϵ -martensite, and continues to change lattice into α' -martensite. The ϵ -martensite does not combine the same strength like the α' -martensite [2, 3].

At the IFUM a deep drawing tool with pins as additional forming elements is created. It allows a free arrangement of different geometries and designs for the generation of martensitic structures in sheet metal. Figure 1 (left) shows different designs of structure fields in EN 1.4301. Aside, the deep drawing tool is pictured with an enlarged detail of the punch. Thereby, the arrangement of pins is demonstrated. The die is equipped with recesses for all possible dispositions of pins in the punch. The structure field comprises martensite contents in the range of about 10% up to a maximum of about 15%, measured by the Feritscope.

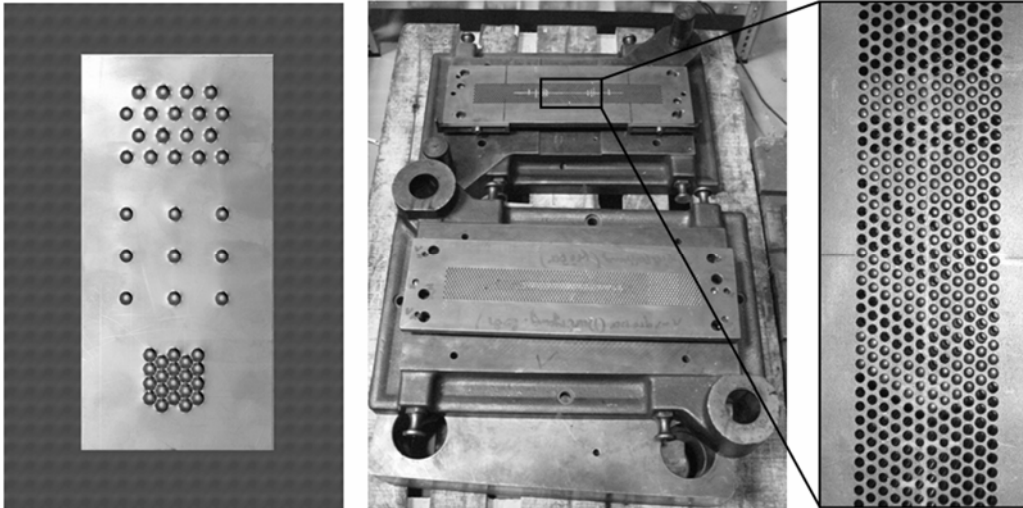


Figure 1. Different martensitic structures in EN 1.4301 (left), produced by additional forming elements in deep drawing tool (right)

One aim of this project is a defined folding of crash components due to the existence of different material properties in one and the same part during deep drawing. Therefore, a carrier demonstrator system has been produced and investigated in crash tests (figure 2). The material behaviour of structured and non-structured demonstrators have been compared. To get more information in detail about the martensitic-austenitic material mixture, Nakajima-tests with structured samples were conducted.

Crash performances of load-adapted components

The crash performance of strain-induced martensitic structures are studied on a z-profile demonstrator for carrier systems with a length of $l = 200$ mm and a width of $w = 53$ mm, shown left in figure 2. To enable a closed contour of this geometry, two parts are joined by using non-vacuum electron beam welding. One aim of this work is the realisation of a defined folding behaviour in the area between martensitic structures. The folding appears while setting up a rabbet of an austenitic ductile region between martensitic high-strength areas. With the martensitic structure fields, the parts are able to absorb more crash energy. The first formation of

folding always takes place between the martensitic structures. The crash performance is mainly influenced due to the combination of two material behaviours in one part. Tests were conducted with a drop impact tester, pictured in figure 2 on the right side. Test parameters are a crash inertia of $m = 100 \text{ kg}$, a crash height of $h = 4 \text{ m}$, a measured velocity of $v = 8.4 \text{ m/s}$ and a total crash energy of $E \approx 3670 \text{ J}$.

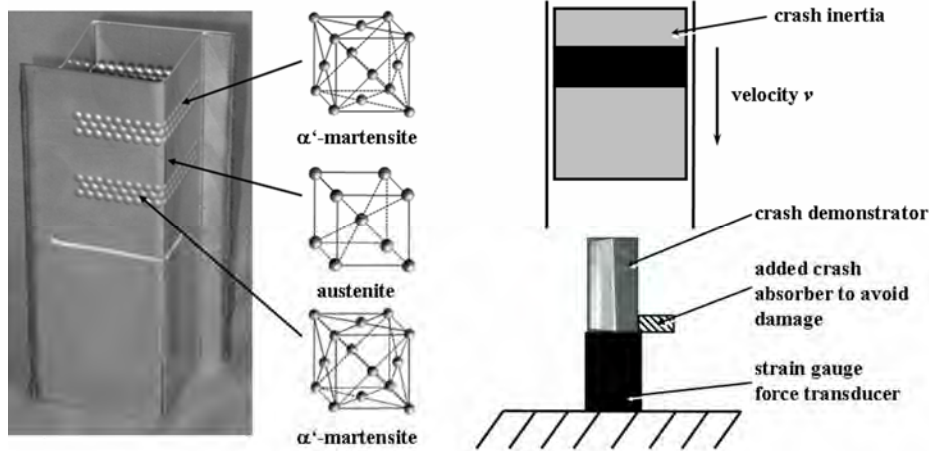


Figure 2. Carrier demonstrator system for crash tests with different material properties (left), assembly of the crash test

The impact on these crash demonstrators are measured with a strain gauge force transducer. After a distance of 160 mm from the first contact of demonstrator top and crash inertia, an emergency deceleration happens due to additional crash absorber. The aim of this test is to prove a defined folding between the martensitic high-strength structure fields. The results are compared with those of a non structured crash demonstrator. Both components are made of stainless steel EN 1.4301 with a sheet thickness about $s_0 = 1.0 \text{ mm}$.

Crash behaviour of a non-structured demonstrator

First crash tests were carried out with a crash demonstrator without martensitic structures in material 1.4301. Figure 3 shows the crash process from beginning till end. The buckling behaviour of this stainless steel is very good due to the high ductility of the austenitic steel. First folding can be seen at the bottom of the demonstrator in the middle picture of figure 3.



Figure 3. Crash process of an unstructured demonstrator from the beginning (left) to the end (right)

Moreover, this tests proceeds with a continuous folding of material. Due to a deformation way of $s_{\max} = 160 \text{ mm}$, the crash inertia is decelerated (figure 3, right). The activating of the emergency stop avoids an onward of folding.

Crash behaviour of a structured demonstrator

In comparison to the previous result, figure 4 shows a crash demonstrator with martensitic structures. Obviously, a defined folding can be achieved due to martensitic structures. In figure 4, the middle picture presents the formation of first folding between the structure fields. The formation of folding starts at the head of the demonstrator and disperses to the bottom. Moreover, due to a deformation way of $s_{\max} = 146$ mm, a deceleration of the inertia is not necessary. Following investigations will specify the influence of martensitic structure fields in these conducted crash analyses in a drop impact tester.



Figure 4. Crash process of a structured demonstrator from the beginning (left) to the end (right)

Summary of the crash performance results

The crash performance behaviour of both components is as good as expected. It can be stated, that the stainless steel EN 1.4301 is adequate for components in crash applications. Moreover, the comparison of both tested structures basically show distinguishable results differing in energy impact, force progression and deformation process. This has been visualised by using a high-speed camera.

The mechanical influence of the crash performance due to martensitic structures is remarkable. The presented crash investigations are very auspicious for further investigations.

Forming Curves (FC) of structured material

To realize load adapted material properties like a better crash performance in the considered steel, the influence of the martensitic high-strength structures on the material behaviour have to be investigated. To research the modification of the material due to martensite evolution and increase in strain-hardening, Nakajima-tests have been accomplished. The chosen design of structures is identical with those seen of the structured crash demonstrator with a pin diameter of $d = 5$ mm and a pin distance of $d_i = 5$ mm. All seven Nakajima-samples have a structure field in the middle according to the design of the crash demonstrator. By the Nakajima-tests a different material behaviour depending on the state of stress is shown. Samples crack at different places, because of the different states of stresses, influenced by sample geometry. They are depending on the occurrence of maximum true strain φ_1 . Due to this, it has been challenging to determine the Forming Limit Diagram. The late cracking of sample 7 influenced by the formation of two φ_1 maxima due to the martensitic structures, adulterate the evaluation of the FLC. Thus, the diagram does not include sample 7 and the range of biaxial stretch-forming (figure 6). Figure 5 shows the local varieties of major true strain exemplary in sample 5. One interesting point is the formation of two local maximums alongside the struture field in the middle of the samples.

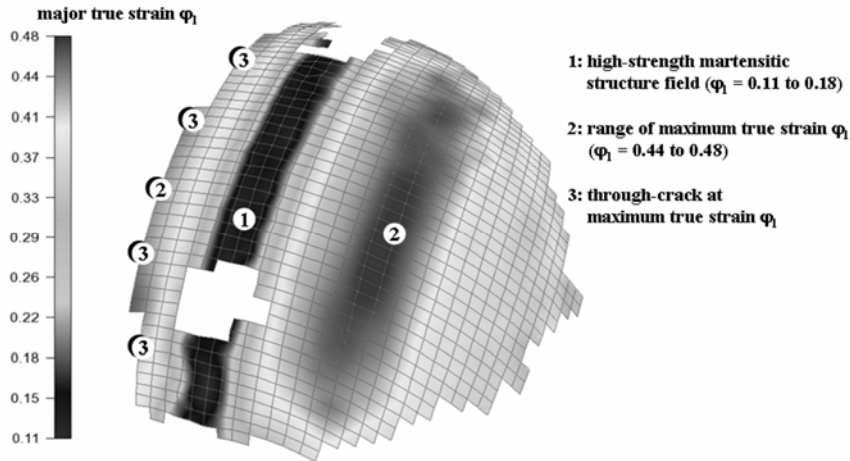


Figure 5. Major true strain distribution of Nakajima-sample 5 after crack

As a result, the gained Forming Curves (FC's) of different material properties are gained for different areas in the samples (figure 6). For an advanced description of the different areas of material behaviour in one and the same part, three curves for different states of strain were plotted.

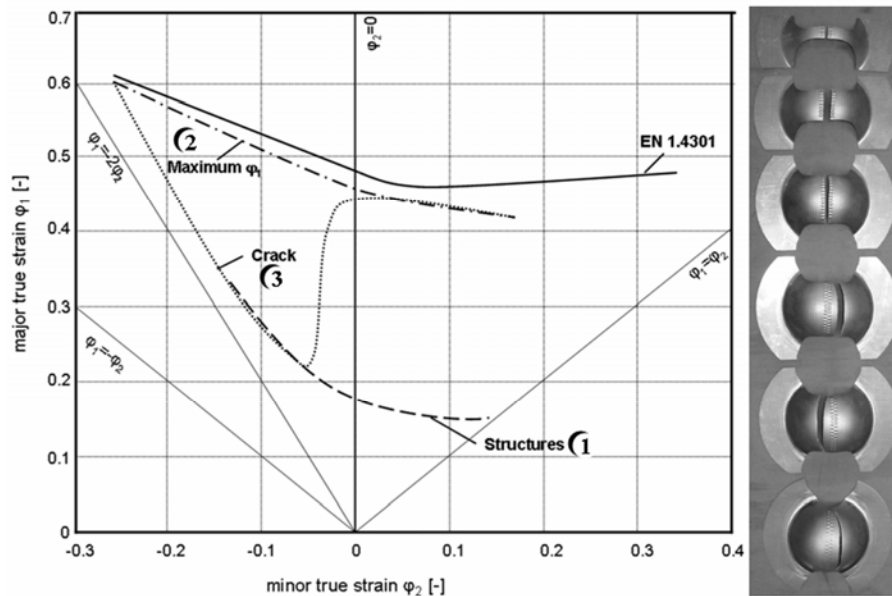


Figure 6. FC's of structured material EN 1.4301 (left) and the cracked Nakajima-samples (right)

Samples do not always crack in the same area, e. g. between the structures or at the maximum major true strain. The curves have been surveyed for the points of the maximum true strain φ_1 , the points of cracks and the points in the middle of the structures of the samples. Due to the three different curves of one and the same material, the combination of different material properties for load-adapted components like crash parts can clearly be seen. Moreover, the austenitic and the martensitic areas in the sample are interacting their material behaviour. For basic orientation, the FLC of the unstructured material EN 1.4301 is shown, too.

Curve 3 describes the crack behaviour of all geometric specimens. Due to the different areas of material failure, this curve does not specify the material behaviour of the martensitic area (Figure 6). The maximum true strain φ_1 is described by curve 2. While influenced by the martensitic structure fields, this curve is lower than the FLC for the material EN 1.4301. All

three curves were determined by the cracked samples. However, it may be possible to represent one FLC for this geometry, but this work emphasises the different states of strains depending on the load-adaption area. The martensitic structure fields were deformed during the Nakajima-tests. Thus, different structure fields in samples exhibit another degree of deformation after tests. It is important to add, that this curves are just effective for this arrangement of structures while the restraint in width direction. The determination of different FC's in this stainless steel demonstrates the local distinctions of material properties due to martensite evolution in austenitic stainless steel. The different material behaviours of the researched areas correlate with the dissimilar states of stresses like plane strain or tensile stress.

Interpreting the curve of crack determined with martensitic structures Nakajima-samples show three areas of this curve. First, at a minor true strain $\varphi_2 = -0.3$ to -0.05 , cracks occur in the zone of martensitic structures in samples 1 to 3. The minor true strain $\varphi_2 = -0.05$ to 0 is the transition zone. The place of crack changes from the middle of the structures to the maximum of major true strain φ_1 . The last area considering in this curve is $\varphi_2 = 0$ to 0.18 . Here, the crack appears at the maximum of the true major strain φ_1 . Moreover, the curve of the crack behaviour shows a good accordance to the curve of the basic material EN 1.4301 in the range of plain strain ($\varphi_2 = 0$) through the biaxial stretch-forming ($\varphi_1 = \varphi_2$).

Conclusion

The good crash behaviour of the stainless steel EN 1.4301 could be upgraded due to the strain-induced martensite evolution. Martensitic structures influence the folding behaviour basically. The gained Forming Curves of the structured stainless steel prove the load-adaption realized by martensite evolution during deep drawing. By the shown structure field the load-adaption for a range of minor true strain $\varphi_2 = -0.05$ to 0.18 could be proved. This work considered the different Forming Curves for different states of strain. Due to this, the determination of the FLC was neglected. Further investigations will deal with more metastable austenitic stainless steels like EN 1.4318 and EN 1.4372.

References

- [1] NGV-Projektleitung: „Edelstahlhersteller zeigen Zukunft des Autos“, Konstruktion 11/12-2007, Springer VDI-Verlag, Germany, p. IW 12, Online: <http://www.ngvproject.org/>
- [2] B.-A. Behrens, K. Voges-Schwieger, S. Hübner: "Non-Destructive Testing for the Determination of Transformation-Induced Martensite in Metastable Austenitic Steels", Proceedings of the IDDRG "Forming the Future - Innovations in Sheet Metal Forming", 21.-23. May 2007 in Győr, Hungary, pp. 93-100
- [3] J. Talonen: "Effect of strain-induced α' -martensite transformation on mechanical properties of metastable austenitic stainless steels", Ph.D. dissertation, Helsinki University of Technology, Finland, 2007.

FATIGUE PROPERTIES OF THIN SHEET STAINLESS STEEL LAP JOINTS

H. Nordberg¹, H.L. Groth²

¹Professor, Formerly head of Outokumpu Stainless Research Foundation, Sweden, ²Outokumpu Stainless AB, Avesta Research Center, Sweden

Abstract

A review of a number of studies performed within the Outokumpu Stainless Research Foundation covering properties of stainless steel overlap joints is presented. The type of joints covered are:

- spot welded stainless to stainless and to galvanised carbon steel,
- adhesive bonded stainless to stainless,
- weld bonded stainless to stainless,
- laser welded stainless to stainless and to galvanised carbon steel,
- clinched stainless to stainless steel.

The materials studied are EN 1.4301 and EN 1.4310 stainless steels and high strength duplex stainless steels with the thickness range 0.7 – 4.0 mm. Fatigue properties in terms of Wöhler curves are compared between the different joining methods using load transfer capacity per unit length of the joints. Fatigue strength is shown to be independent of material strength for spot welded joints. Spot welded, laser welded and clinched joints show similar fatigue properties for 1 mm sheet joints. Adhesive bonded joints are five-fold stronger and the weld bonded joints show considerable scatter with a lower bound fatigue strength between spot welded and adhesive bonded joints.

Introduction

Structural applications represent one of the fastest growing segments for stainless steel. In the US market some 20 percent of all stainless steel is estimated to be used in this market sector. A good example of a growing sub-segment is the transportation, e.g. in busses and trains. It is not only the corrosion resistance of stainless steels, which is of interest. To further increase the penetration of this market it is important to develop our understanding of the mechanical properties of stainless steel and stainless steel structural elements. This implicates, among other things, a need to develop joining techniques suitable for these applications, to establish the behaviour of structural elements under static and dynamic loads and to develop design guides. In the basic mill-annealed condition stainless steel grades are available with typical yield strengths ranging from 260 to 620 MPa. In the temper rolled (cold rolled) condition, grades are available with yield strengths of from 350 to over 2000 MPa. The high strengths available will lead to lighter, more slender structures based on thin sheet panels, shells and members in general. The thin sections will call for new and innovative techniques for fabrication and joining of members. Traditional butt welding techniques will still be used but the thin section will make it feasible to join with other methods using overlap type of joints.

In the present paper, a number of overlap joining methods are considered with special focus on the fatigue properties of such joints. Most of the results presented are results from a series of PhD studies financed by Outokumpu Stainless Research Foundations in a long term program to increase the knowledge on thin sheet joining techniques [1]. Also some data from the “Light and safe”-project [2] has been added in the results presented.

Single-Overlap Joint

The basic type of overlap joints is schematically shown in Figure 1. The joining technique is assumed to be adhesive bonding but could as well be spot welding, laser welding, clinching, riveting or a combination of these. The single lap joint with some modification is for obvious reason the most widely used.

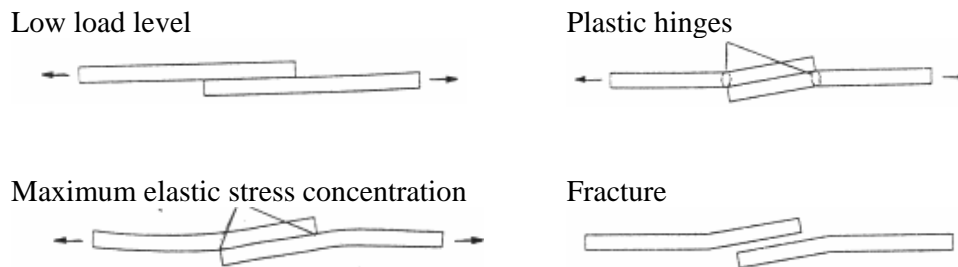


Figure 1. Deformation of single over-lap joint during loading.

Rotation of overlap joints.

The eccentricity of the load path, results in a rotation of the joint during loading. This will result in a tensile load (Mode I) in combination with the shear load (Mode III). This effect has been demonstrated a number of times over the last half century. The first analytical solution to show this was made by Goland & Reissner [3] in 1950's.

Lap joint load transfer capability.

In most engineering research reports the tensile and fatigue strengths are given in terms of net section stress. This is the case also for continuous butt joints. For spot welded joints there seems to be no general rule. Some reports give total load and define the number of spot welds, others report the strength as the net section stress of the specimen tested and still others have reported strength as the corresponding shear stress on the nugget.

To be able to compare the properties of different joining techniques the strength of the joints will be given both as the net section stress on the thinner of the two sheets joined and as the “line load”, Q , i.e. the load divided by the width of the joint. Dividing the line load with the thickness then gives the net section stress.

For discontinuous joining techniques (e.g. spot welding, riveting, clinching) the width of the joint has to be defined for each technique. In the following the optimal distance between the closest two spot welds, the “pitch”, will be calculated by Eq. (1):

$$e = (14 \cdot t_2 + 3) \cdot \sqrt[3]{\frac{t_1}{t_2}} \quad \text{where } t_1 \geq t_2 \quad \text{Eq. (1)}$$

For a spot welded joint the line load is thus calculated as load per nugget divided by the pitch calculated by the equation above.

Materials

The nominal chemical compositions of the materials in this paper are given in Table 1.

Table 1. Nominal chemical compositions (wt.%) of materials studied. LDX 2101[®] is an Outokumpu registered trade mark

Material	C	Cr	Ni	Mo	Mn	Other
EN 1.4301	0.02	18	9			
EN 1.4310	0.10	17	7			
EN 1.4401	0.02	18	12	2.5		
LDX 2101 [®]	0.02	21	1.5		5	N
2304	0.02	23	4			N
2205	0.02	22	5	3		N

Fatigue properties – Spot welded joints

The fatigue properties of spot welded joints of stainless steel sheets range from 6 to 60 MPa compared with the bulk fatigue properties of 250 to 400 MPa. This poor fatigue strength demonstrates the importance of a reliable design tool for spot welded joints. Linder et al [4, 5] (among a lot of other researchers) suggested a fracture mechanics approach for the analysis of the results. The basis for this was that the two sheets create a crack with the tip at the weld nugget. Stress intensities around the weld nugget for Mode I-III could be calculated in order to find the maximum stress intensity and its location.

The result from this calculation is presented in the form of an effective stress intensity factor, K_{eff} , defined in [4] as: $K_{eff} = (K_I^2 + K_{II}^2 + K_{III}^2 / (1 - \nu))^{1/2}$.

For single overlap joints, K_{eff}^{max} , is located in the loading axis direction where fatigue cracks were observed to initiate. If all failed specimens were recalculated using K_{eff}^{max}/P , where P is the applied load. The stress intensity ranges, $\Delta K = \Delta P * (K_{eff}^{max}/P)$, versus number of cycles to failure for all specimen types, thickness and grades are shown in Figure 2. Data from Refs. [4-7].

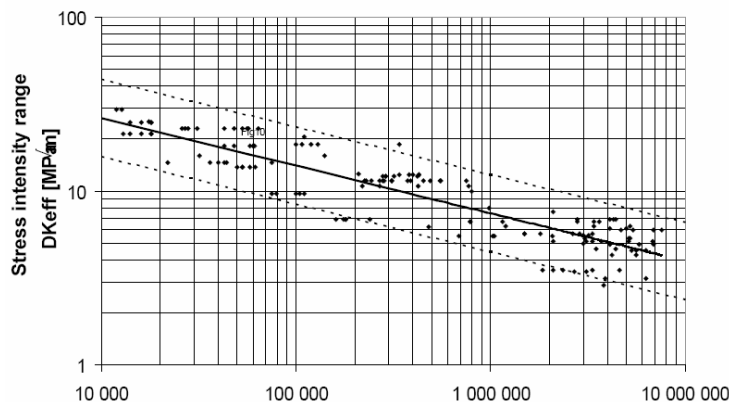


Figure 2. Stress intensity ranges versus number of cycles to failure for all specimen types, sheet thickness and steel grades. 95% confidence limits are shown.

From Figure 2 it is evident that the spot welded joints are a fracture mechanics problem and that it could be described and understood using this technique. Fatigue strength is independent of

material strength for spot welded joints. Spot welded and projection welded joints show similar fatigue strength.

Fatigue properties - Adhesive joints

Boyes [8] tested box-type specimens with a 40 mm overlap using 4 mm gauge EN 1.4301 material. In figure 3 his results using the stiff “Box” specimen are compared with results from testing of single overlap joints with 1.5 mm gauge sheet and with two bondline thicknesses. The load range is given as load per unit length of the joint.

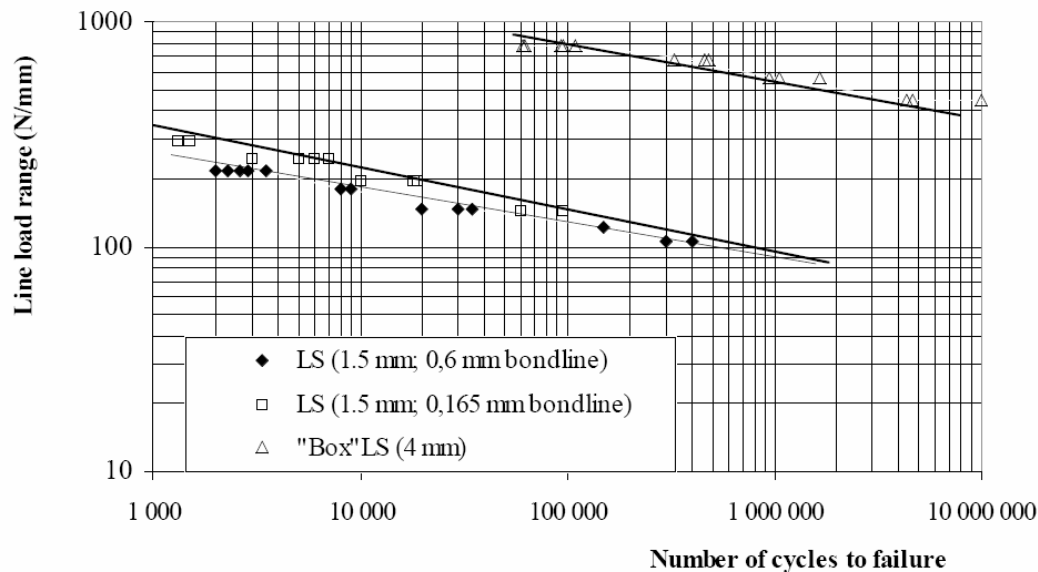


Figure 3. S-N curve for 4 mm flanged specimen and 1.5 mm specimen overlap joint in grade 1.4301.

For the 4 mm thick material using the stiff “Box” specimen the fatigue strength at 10^6 cycles is estimated to be 500 N/mm compared with 80 N/mm for the thinner material in the overlap joint configuration. For longer lives the increased bondline thickness does not affect the strength. Although results in Refs. [8-10] from dry air testing indicate a dramatic increase in fatigue strength going from spot welding to adhesive bonding, a number of questions about adhesive bonding have to be resolved. The long term behaviour and the effect of different environments on bonded joints needs special attention.

Fatigue properties - Weldbonded joints

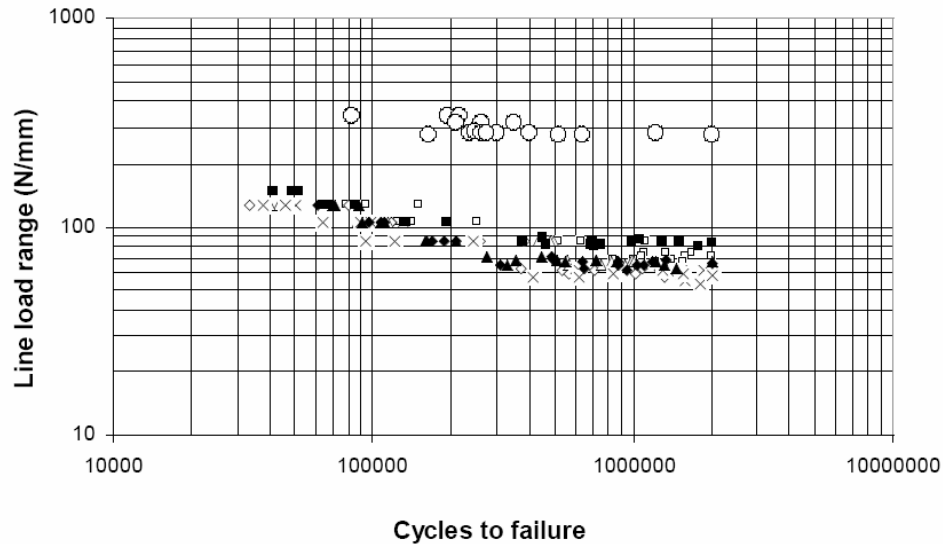
Results given in Refs. [5, 8-10] together with the results from identical specimen type for both spot welding and adhesive bonding shows that the fatigue limit for weldbonded joints is estimated to be approximately twice that for spot welded joints but less than half of that for adhesively bonded joints.

Fatigue properties - Laser welded joints

Compared to spot welding, laser welding can be done continuously, drastically reducing the stress concentrations in the joint as discussed by Kaitanov [11]. Dinsley [12] studied laser welded overlap joints between stainless steel and galvanised carbon steel.

Linder et al. [13] have tested laser welded cold-worked EN 1.4301 (304). For shorter lives they showed that an increase of weld width for 1.0 mm sheet joints from 0.6 to 1.3 mm increased fatigue strength by about 30 %. At the same weld width the strength increased by 75 % with increasing sheet thickness to 2.5 mm.

A summary of the results from Refs. [11-13] is given in Figure 4. It can also be noted that a wider weld increases the fatigue strength. The fatigue strength in terms of line load range is almost linearly related to the sheet thickness at similar weld width. This means that the nominal net section stress range is equal at about 60 MPa. (This may be compared with duplex LDX 2101[®] butt weld with fatigue strength of 278 MPa.) V1437 is a carbon steel.



□ 1.2mm V1437(top)-1mm 304 Lap weld	◇ 1mm 304 (top)-1.2mm V1437 Lap weld
△ 1.2mm V1437 (top)-0.78mm 2205 lap weld	× 0.78mm 2205 (top)-1.2mm V1437 lap weld
■ 1mm LDX2101 lap weld	▲ 1.2mm V1437 (top) - 1mm LDX2101
◆ 1.2mm V1437 (top) - 1mm 2205	○ 1mm LDX2101-1.2mm V1437 butt weld

Figure 4. Fatigue properties of laser welded overlap joints.

Fatigue properties – Clinched joints

So far most of the experience is with soft, mild steel and aluminium alloys in the automotive sector. The response given by stainless steel, with their characteristic strong deformation hardening and high ductility, have to be investigated to establish the limitations for clinching. Fatigue of clinched stainless steel joints have been reported by Jacobsen [14]. Since clinching introduces large plastic deformations in the clinched area, a less stable EN 1.4301 (CrNi 18-10) and the more stable version (CrNi 18-12) were tested and results are shown in Figure 5.

Sjöström [15] tested three grades with different austenite stability; EN 1.4310, EN 1.4310 and EN 1.4401, all annealed. As opposed to [14] for round clinch the fatigue properties increases rapidly with increasing degree microstructural stability and decreasing strength for the rectangular clinch. The fact that rectangular clinches contains macrocracks (clinch size) normal to the loading direction could explain the different response to the strength in the deformed (clinched) area. Round clinched joints have about twice the fatigue strength of the rectangular clinched joints.

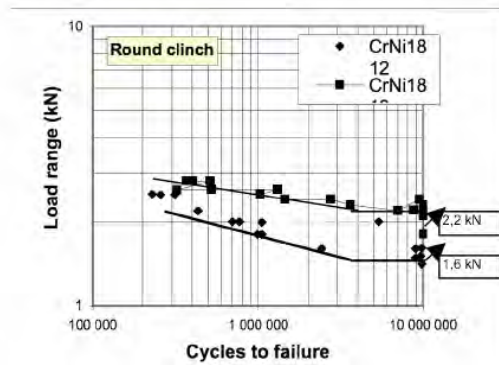


Figure 5. S-N curves for 1 mm clinched lap shear joints, grade 1.4301 with two different Ni-levels.

Summary

- Fatigue strength is shown to be independent of material strength for spot welded joints.
- Spot welded, laser welded and clinched joints show similar fatigue properties for 0.8 – 1.5 mm sheet thickness of about 70 N/mm.
- Adhesive bonded joints are five-fold stronger compared to spot welded joints.
- Weld bonded joints show a fatigue strength between spot welded and adhesive bonded joints.

References

- [1] Nordberg, H., "Fatigue Properties of Stainless Steel Lap Joints", SAE paper 2005-01-1324.
- [2] Final Technical Report, "Light & Safe - Weight Reduction for Safer, Affordable Passenger Cars by using extra Formable High Strength Austenitic Steel", European Community under the 'Competitive and Sustainable Growth' Programme, 2005.
- [3] Goland, M. and Reissner, E.J., Appl. Mech., 1944, Vol. 2, p. A-17.
- [4] Linder, J., et al., Swedish Institute for Metals Research, Report IM-3475, 1997.
- [5] Linder, J., et al., "Fatigue Data and Design Methods for Spot Welded Austenitic and Duplex Stainless Sheet Steels". In "Stainless Steels in Transport Industry". Espoo, Finland, 1998.
- [6] Wray, T., "Resistance Spot Welding Of Duplex Stainless Steel", PhD Thesis, Sheffield Hallam University, 2004.
- [7] Marples, M., PhD programme. Sheffield Hallam University, 2002.
- [8] Boyes, R., "Adhesive Bonding of Stainless Steel; Strength and durability". PhD thesis, Sheffield Hallam University, 1998.
- [9] S.McCann, S., PhD programme. Sheffield Hallam University, 2003.
- [10] Ring-Groth, M., "Adhesive Bonding and Weldbonding of Stainless Steel," Lic. thesis, Luleå University of Technology, Luleå, 1998.
- [11] Kaitanov, A., "Static and Fatigue Strengths of Laser Welded Over- Lap Joints with Controlled Penetration". Progress Rep., State Univ. of Marine Tech., St.Petersburg, 2002.
- [12] Dinsley, C., Laser Welding of Austenitic and Duplex Stainless Steel to Zinc-Coated Mild Steel. PhD thesis, Sheffield Hallam University, 2004.
- [13] Linder, J., et al., "Fatigue Strength of Laserwelded Stainless Steel Sheets", Swedish Institute for Metals Research Report IM-2000-529.
- [14] Jacobsen, J., "Beitrag zum umformtechnischen Fügen von Stahlblechteilen mit vorwiegend Austenitischem Gefüge", Tech. Univ. Hamburg-Harburg, Dr.-Ing Dissertation, 1997.
- [15] Sjöström, P., to be published, Linköping University, 2004.

WELDING STAINLESS STEELS – PRACTICAL RESPONSES TO REGULATORY TRENDS

D. Jordan

Consultant to the Nickel Institute, UK

Abstract

Welding of stainless steels is affected by regulatory trends towards reduction of limits for exposure to welding fume. The physical and chemical characteristics of welding fume are described and concerns about possible health hazards are explained. The nature of the response by authorities in different countries shows the need for industry to take positive steps to accommodate stringent regulations. Practical measures to manage the changing situation are outlined.

Introduction

Arc welding and allied processes generate particulate fume, which has the potential to affect the health of welders and others, if inhaled. Occupational health authorities therefore define limits to the concentration of fume in the workplace, not only in total but also in terms of the individual constituents that make it up. Filler metals for stainless steels contain chromium, nickel and manganese, compounds of which are subject to control under the regulatory regime. The purpose of this paper is to define the characteristics of stainless steel welding fume, to review trends in regulations, and to suggest the response that is required to meet changing demands.

Characteristics of welding fume

Physical characteristics

Almost all welding fume is generated by the filler metal; little originates from the austenitic or duplex stainless steel being welded. It is formed by a mechanism involving vaporisation, oxidation and condensation. Particles are very small: in an early study [1] of fume produced by an E308-16 flux-coated electrode it was found that they were individual spheres or clusters of spheres that had been fused at high temperature; 75% were smaller than 0.2 μm , 24% smaller than 0.4 μm , only 0.2% larger than 1.0 μm . Comparable results were obtained for fume generated during plasma cutting of austenitic and duplex stainless steels [2] and for tungsten inert gas welding [3].

Chemical composition

An analysis [1] of welding fume from a flux-coated stainless steel electrode is compared with a typical weld metal composition in Table 1.

Table 1. Chemical composition of MMA stainless steel weld metal and fume

AWS A5.4 E308-16	Mass %							
	Fe	Si	Mn	Ni	Cr	K	Na	F
Weld metal*	Bal.	0.6	1.0	9.5	19.0	-	-	-
Fume [1]	10.8	4.9	6.20	0.75	5.6	18.9	10.4	16.8

* Manufacturer's typical data

The proportions of the alloying elements differ from those in the weld metal due to variations in their vapour pressure; thus manganese is over-represented and nickel is under-represented. Fume particles are complex. Advanced techniques have been used [4] to show a core-shell structure formed by the different condensation temperatures of the elements within the fume. Particles of $K_2(Cr,Mn,Fe)O_4$ were enclosed in coatings formed from elements in the flux covering, particularly SiO_2 . The presence of hexavalent chromium compounds is typical of flux-shielded processes.

In the absence of flux effects, the composition of welding fume generated during gas-shielded metal arc welding more nearly reflects the composition of the filler wire:

Table 2. Chemical composition of GMAW stainless steel weld metal and fume

AWS A5.9 ER316LSi	Mass %					
	Fe	Si	Mn	Ni	Cr (total)	CrVI
Fume	39.5	0.96	14.6	3.7	16.4	0.17
Wire*	Bal.	0.8	1.4	12.8	18.5	-

* Typical analysis – manufacturer's data

A particularly noteworthy characteristic of fume from gas-shielded welding processes is the small fraction of the total chromium content in the hexavalent form. Nickel is in the form of spinels such as $NiFe_2O_4$ [5]. The core-shell structure appears to be less common in this type of fume.

Hazards

Since welding fume particles generally fall within the respirable range [6], they are capable of entering the deepest parts of the lungs and therefore a main focus of investigation has been the potential for lung cancer among welders. For stainless steel welding fume, the presence of hexavalent chromium compounds is a cause for concern because they are classified as *carcinogenic to humans* (Group 1) by the International Agency for Research on Cancer, while trivalent chromium compounds are *unclassifiable as to carcinogenicity to humans* (Group 3). Nickel compounds are also classified in Group 1. More recently, attention has turned to manganese, which has been found to cause neurological disorders in workers in industries processing manganese and manganese compounds.

Risks

The possibility of long-term effects on the health of welders from inhalation of welding fume has been explored in a number of epidemiological studies. The most extensive of these was the IARC review [7], which concluded that there was evidence of excess mortality due to lung cancer in welders of all types of steels. However, the excess mortality could not be related to cumulative exposure to total fume, total chromium, hexavalent chromium or nickel. Subsequent epidemiological surveys have produced conflicting results with no conclusive evidence for a difference in morbidity between welders of carbon steels and welders of stainless steels. The

presence of asbestos in the workplace has been cited by some investigators as the cause of the excess risk [8]. There appears to be no clear evidence at present of any influence of manganese in welding fume on the health of welders [9].

Exposure regulations

Table 3 shows exposure limits for total welding fume and for individual components fume generated in welding stainless steels.

Table 3. Current exposure limits for total welding fume and constituents

Country	Standard/Limit	Substance mg/m ³				
		Total fume	CrVI	CrIII	Ni (insol.)	Mn
UK	Workplace Exposure Limit (WEL)	(5)*	0.05	0.5	0.5	0.5 ¹ (1)
Germany ²		3 ¹	(0.1/0.05)	-	-	-
Netherlands	Maximum Allowable Concentration (MAC)	3.5	0.025	0.5	1.0	1.0
Sweden	Occupational Exposure Limit (OEL)	5	0.005 (0.02)	0.5	0.1	0.1 ¹ (0.2)
USA	Permitted Exposure Limit (PEL)		0.005 (0.05)	0.5	1	5

* Figures in brackets previous limits ¹respirable

²No limits for individual substances available under a 2004 ordinance (Gefahrstoffverordnung)

There is little consistency in the concentration limits specified in different countries: in part this is due to variation in how the available data on the toxicity of a particular substance are evaluated, in part because some authorities are required to take economic factors into account when defining the limit. Revision dates also vary.

It is important to note that, apart from limits for exposure to total fume, these regulations apply to exposure from a variety of sources and in different industrial environments. For example, the 2006 US standard [10] for exposure to hexavalent chromium was the result of a critical review of data on the health of workers as affected by inhalation of mists, dusts and fumes in applications as diverse as alloy production, painting, electroplating, and welding. Thus the substances discussed here are classified by valency and solubility rather than as specific compounds.

Conformity

Calculation shows that the proportion of an individual component of stainless steel welding fume governs its allowable concentration, rather than the total fume limit. Thus, for manual metal arc fume containing 5% CrVI, 5% Mn and 1% Ni, the maximum permissible fume concentration would be 1 mg/m³ in the UK or 0.1 mg/m³ in Sweden, based on the 'key' component, hexavalent chromium. Protective measures are therefore more demanding than for low-alloy steels.

A hierarchy of controls is often followed to manage risk, such as the following:

1) Elimination; 2) Substitution; 3) Engineering controls; 4) Administrative controls; 5) Personal protective equipment.

If welding is essential, as is usually the case, level 2) suggests the replacement of flux-based arc processes (except submerged-arc welding) by gas-shielded processes, to avoid formation of hexavalent chromium compounds. While chromium is indeed present in trivalent form, nickel may supplant it as the key component, e.g. in Sweden, giving a maximum total fume concentration of

less than 1 mg/m³. The gas-shielded tungsten arc process, in which the arc is not formed with the filler wire, produces very little fume. Processes are primarily selected for technical and economic reasons, however, and so the scope for substitution is relatively small.

Engineering controls form the main means for restricting exposure, primarily through general and/or local ventilation. An analysis [1] of exposure to fume generated by 308L stainless steel consumables under controlled conditions in which, with a duty cycle of 20%, total fume exposures of 0.1 mg/m³ or less were only obtained when the welder's head was infrequently within the fume plume and local exhaust ventilation was used. While published individual data concerning fume from stainless steel welding are relatively sparse [12], in an extensive survey of exposure to hexavalent chromium in shipyards [13], it was found that local exhaust ventilation did not significantly reduce exposure, compared with general ventilation. In contrast, controlled laboratory tests showed that it was effective when properly used, pointing to the difficulty of ensuring that controls are fully operative under workplace conditions.

There are limited opportunities to control exposure through administrative arrangements. For example, since the exposure limit usually relates to an 8-hour time-weighted average, the time a worker spends during a shift in welding could be restricted by rotating jobs.

Personal protective equipment, such as helmets fitted with filters or air-fed helmets offers an attractive means of protection, though it should only be considered when the benefits of higher-level controls have been exhausted. Nevertheless, helmets must be worn continually to be fully effective and the degree of protection they offer diminishes rapidly if they are removed for even short periods [14]. In some circumstances, it may also be necessary for ancillary personnel to be provided with protection.

Discussion

Conformity with the relevant regulations poses a range of problems for fabricators: they have a duty to assess the risk to which their welders are exposed and then to take measures to protect them. Initially, fume exposure must be measured; in some cases, this will entail monitoring all exposed employees [10] - clearly a relatively expensive and time-consuming operation, particularly for the small and medium-sized workshops that form a significant proportion of fabrication businesses. They must then formulate a plan for protection that will minimise the risk or at least reduce it to a level that is acceptable under the relevant regulations.

A survey [15] of users of hazardous substances in the UK found that most relied on commonsense judgements when making risk assessments and only a relatively small minority made measurements of atmospheric concentration. It is therefore helpful that some national regulatory bodies are publishing guidance notes to show what measures have to be taken to give reasonable assurance of conformity with exposure limits. For example, guidelines have been published in The Netherlands [16], drawn up on the basis of measurements made in welding workplaces. They take into account the concentrations of key components in the breathing zone of the welder, duty cycle, and the process-material combination. For example, no special precautions are required when welding stainless steels by the TIG process while a separate ventilated space is specified when the MMA or GMAW process is used, along with the use by the welder of a filter unit helmet or air-fed helmet. In the UK, as part of a regime [17] in which the MEL Maximum Exposure Limit and OES (Occupational Exposure Standard) have been replaced by the single WEL (Workplace Exposure

Limit), detailed information on good practice has been published as leaflets for employers and employees and on a web site. However, these two examples are the exceptions and fabricators have no resource of data to relate levels of exposure to different fume components to appropriate protective measures.

Up to the present, the fabrication industry has reacted slowly to the challenge of new and more demanding exposure limits. For example, a survey [18] showed that a substantial proportion of Swedish fabricators of stainless steels were unprepared to meet the requirements of the current limits for hexavalent chromium and manganese, only months before their introduction. In the USA, OSHA has agreed to allow a period of four years for the development and implementation of the engineering controls needed for compliance with the hexavalent chromium standard after its introduction in 2006. Recognising that occupational health will no longer be an ancillary activity in future, but will be an important consideration in planning welding operations, there is a need for positive research and development in anticipation of the difficult times ahead.

References

- [1] American Welding Society. 1983. Characterisation of arc welding fume.
- [2] Lillienberg, L. and von Brömssen, B.: 1997. The Swedish Institute of Production Engineering Research.
- [3] Farrants G, Schuler B, Karlsen J, Reith A, Langard S.: Am. Ind. Hyg. Assoc. J. 50(9): 473-9.
- [4] Sowards, J.W.: IIW Document No. VIII-2018-06.
- [5] Lausch, H.: 1999. Abschlussbericht zum Forschungsvorhaben. pub. HVBG, Germany.
- [6] ISO 7708: 1995. Air quality – Particle size definitions for health-related sampling.
- [7] International Agency for Research on Cancer. IARC Monographs; Vol. 49.
- [8] Becker, N.: 1999. JOEM, 41, 4, 294-303.
- [9] McMillan, G., Spiegel-Ciobanu, V.E.: 2007. Welding and Cutting 6 (4), 161-165, 220-229.
- [10] OSHA. 2006. Occupational exposure to hexavalent chromium; Final Rule.
- [11] Carter, G.J.: 2004. Welding and Cutting (DVS), 3 (6), 364-371.
- [12] TWI. 2003. Fume exposure database.
- [13] US Navy/Industry Task Group. 1995. Impact of Anticipated OSHA Hexavalent Chromium Worker Exposure Standard on Navy Manufacturing and Repair Operations.
- [14] Balieu, E.: International Conference: Health and Safety in Welding and Allied Cutting Processes, 2005.
- [15] Industry's perception and use of occupational exposure limits. 1997. Health and Safety Executive. 1997. Contract Research Report 144/1997.
- [16] Praktijkrichtlijn 'Beschrijving doeltreffende maatregelen bij blootstelling aan rook en/of gassen afkomstig van lassen en/of verwante processen'. 2006..... Ministry of Social Affairs and Employment, The Netherlands.
- [17] The Control of Substances Hazardous to Health (Amendment) Regulations 2004. Statutory Instrument 2004 No. 3386. pub. HMSO.
- [18] Gavelin, F. IIW Document VIII-2029-06.

ALLOYING CONCEPTS FOR LEAN DUPLEX STAINLESS STEEL WELD METALS

L. Karlsson, C. Gillenius, H. Arcini, E.-L. Bergquist

ESAB AB, Sweden

Abstract

Effects of alloying with Mn in combination with different levels of N, Ni and Cr were explored for lean duplex weld metals. Focus was on finding compositions producing a minimum PRE_N value of 25 while at the same time fulfilling typical requirements on weld metal mechanical properties. A number of experimental covered electrodes were developed and corresponding weld metal microstructures and properties were evaluated. Strength, ductility and PRE_N requirements were readily matched. However, both a fully ferritic solidification, producing a typical duplex weld metal microstructure, and a sufficient Ni-content were necessary to produce acceptable and reproducible impact toughness at room and sub-zero temperatures. It was concluded that a composition of 23-24%Cr, 7-8%Ni, 0-0.3%Mo and 0.12-0.16%N was well suited to fulfil requirements.

Introduction

Duplex stainless steels nowadays comprise a large family ranging from the lower alloyed lean grades, that are cost efficient and compete with the standard austenitic grades, to the highly alloyed superduplex and hyperduplex grades for more demanding applications [1-3]. Some of the Ni in modern lean duplex stainless steels is typically replaced by a combination of Mn and N in order to keep the alloying cost at a minimum while maintaining strength, corrosion resistance and a suitable phase balance. The recent rapid increase in Ni- and also Mo-price have made these steels very interesting as alternatives to austenitic grades.

There is no clear-cut definition of what is to be considered as lean duplex stainless steels (LDSS). It has been proposed that “lean” should be reserved for almost Mo-free grades with a Ni-content lower than 3% [4]. Using this definition neither 32003 nor 32304 would be termed lean (Table 1). From the welding point of view a slightly different approach can be taken. Looking at mechanical properties and corrosion resistance it is clear that all duplex grades leaner than standard 22%Cr duplex can be welded with 2209 type consumables (22Cr 9Ni 3Mo 0.15N). There are basically two reasons for using a consumable with a composition more closely matching the leaner steel grades. Firstly there is an obvious cost advantage if Ni- and Mo-content can be decreased and secondly there are some applications where Mo has a negative effect on corrosion resistance. It therefore makes sense to develop consumables matching properties of lean grades with no or little Mo, such as 32001, 32101 and 32304 (Table 1), treating the Mo-containing grade 32003 separately.

Welding consumables for duplex stainless steels need to be higher in elements promoting austenite formation, compared to the corresponding steel grade, to avoid excessively high weld

metal ferrite contents. At the same time it is important to ensure appropriate mechanical properties and corrosion resistance. Weld metal design therefore requires a careful balancing of

Table 1. Typical chemistry of some stainless steels.

Steel type	AISI/UNS	EN	Cr	Mo	Ni	Mn	Cu	N	PRE	PRE _N
Austenitic	304L	1.4307	18	0	9	1	0		18	18
	316L	1.4401	17	2	11	1	0		24	24
	904LN	1.4339	20	4	25	1	1.5	0.1	33	35
“Lean” duplex	S 32001		20	0.3	1.7	5	0.3	0.15	21	23
	S 32101	1.4162	21	0	1.5	5		0.2	21	24
	S 32304	1.4362	23	0	4	1		0.13	23	25
	S 32003		20	1.7	3.5	2		0.15	26	28
22%Cr duplex	S 32205	1.4462	22	3	6	1		0.17	32	35

PRE = %Cr + 3.3%Mo, PRE_N = %Cr + 3.3%Mo + 16%N

alloying elements. The more recently introduced LDSS (32001 and 32101) are both rather high in Mn and N whereas the older 32304 grade is higher in Cr and Ni. Possibilities and limitations of alloying welding fillers with Mn in combination with different levels of N, Ni and Cr were therefore explored for lean duplex compositions. Focus was on finding compositions with 20.5%Cr to 24%Cr for N-levels producing a minimum PRE_N value of 25.

Experimental

In these experiments it was decided to study selected combinations of Mn, Ni, N and Cr covering composition ranges of interest for the three Mo-free lean steel grades presented in Table 1. A number of specially designed covered electrodes were therefore developed to complement previous studies on lean duplex GMAW weld metals produced with experimental metal-cored wires [5] and to widen the range of compositions studied.

Thermodynamic calculations

The phase equilibrium of potential weld metal composition was calculated using the ThermoCalc software [6] to select compositions of interest. Figure 1 shows an example of an isopleth for N-contents between 0 and 0.3 % for 5% Mn suggesting that high temperature nitride precipitation should not be expected but that some austenite might form during solidification, in particular at higher N-levels.

Welding and testing details

Twelve Manual Metal Arc (MMA) all-weld metals were produced at a heat input of approximately 0.9-1.1 kJ/mm and with a maximum interpass temperature of 150°C. Welds were deposited in buttered ISO-joints using 2.5 or 3.2 mm diameter electrodes in 15 mm plate material or with 4 mm electrodes in 20 mm plate material. Weld metals were subjected to metallographic studies, chemical analysis and mechanical testing. Tensile test specimens were machined from the centre of the joints in the longitudinal direction. Charpy-V (10x10 mm) specimens from weld metal centre were

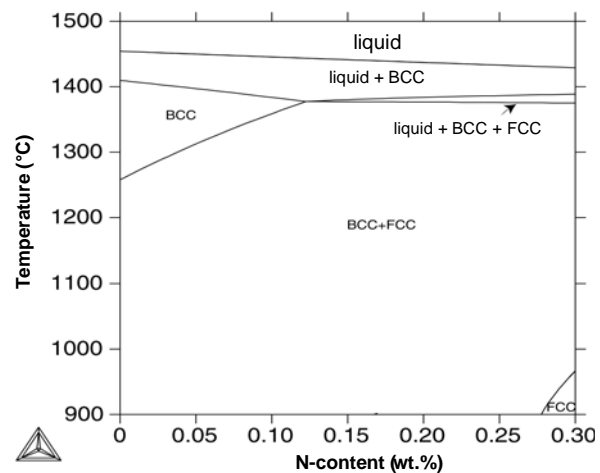


Figure 1. Isopleth calculated by ThermoCalc [6] varying N between 0 and 0.3 wt.% for a base composition of (in wt.%) 0.02 C, 0.7 Si, 5.0 Mn, 21.7 Cr, 4.0 Ni, and 0.5 Cu.

tested at room temperature, at -20°C and for most welds also at 0°C and -40°C. Cross-sections were prepared for examination of the microstructure by grinding and polishing to 1 µm diamond solution. The samples were then either electrolytically etched in 40% KOH or etched using Berahas colour etchant. Microstructures were studied by light optical microscopy (LOM). The ferrite content was quantified by measuring the Ferrite Number (FN) using a Fischer Feritscope. The chemical composition of weld metals was determined using optical emission spectroscopy and LECO combustion equipment for C, S, O and N.

Results

Chemical analysis

As presented in Table 2 weld metal Mn, Cr, Ni and N contents were varied while the concentrations of other elements remained practically constant. The exception was weld metal 7 that in addition was alloyed with 0.35 % Cu. The aimed minimum PRE_N value of 25 was reached for all except weld metals 10-12.

Table 2. Chemical composition (wt.%) and PRE_N of experimental MMA lean duplex welds.

Element	Weld											
	1	2	3	4	5	6	7	8	9	10	11	12
C	0.030	0.027	0.041	0.044	0.05	0.03	0.05	0.03	0.03	0.04	0.04	0.03
Si	0.80	0.76	0.80	0.85	0.91	0.94	0.78	0.58	0.69	0.71	0.72	0.56
Mn	0.96	0.95	5.1	4.9	4.90	0.99	0.77	3.03	3.84	4.87	5.12	2.89
Cr	23.5	23.6	21.7	21.7	20.7	23.7	23.5	22.8	22.9	20.7	20.8	20.5
Ni	8.9	8.8	5.7	3.6	3.5	8.8	7.3	5.2	5.1	4.5	4.6	4.8
Mo	0.05	0.05	0.01	0.01	0.26	0.29	0.25	0.33	0.31	0.31	0.31	0.34
O	0.07	0.07	0.07	0.07	0.06	0.09	0.11	0.07	0.07	0.06	0.05	0.06
N	0.18	0.14	0.25	0.25	0.26	0.17	0.14	0.19	0.19	0.13	0.16	0.18
PRE _N	26.5	26.0	25.7	25.7	25.7	27.4	26.6	26.9	27.0	23.8	24.4	24.5

$$(PRE_N = Cr + 3.3Mo + 16N)$$

Mechanical properties

The tensile strength was well above 700 MPa for all weld metals with the highest level for those high in N and Mn (Table 3). Yield strength varied between 545 MPa and 805 MPa again with the highest level measured for a Mn-alloyed high-N variant. Impact toughness varied significantly with values ranging from 31 J to 106 J at room temperature and from 8 J to 58 J at -20°C (J).

Table 3. Tensile properties and Charpy-V impact toughness of experimental lean duplex all-weld metals.

Property	Weld											
	1	2	3	4	5	6	7	8	9	10	11	12
Rp _{0.2} (MPa)	545	599	-	-	805	758	632	-	646	612	649	673
R _m (MPa)	716	777	773	810	820	779	788	798	807	774	809	807
A ₅ (%)	34	28	31	27	26	28	25	26	28	28	26	24
Kv at +20°C (J)	46	62	56	31	37	61	63	75	72	103	95	106
Kv at 0°C (J)	-	-	-	-	-	-	52	46	44	67	51	83
Kv at -20°C (J)	38	52	26	8	8	53	48	31	33	40	32	58
Kv at -40°C (J)	-	-	-	-	-	-	42	19	17	23	15	40

Microstructure

The welds could be divided into two groups according to their microstructural morphology (Figure 2 and Table 4). Seven of the welds had a typical duplex weld metal microstructure throughout (Figure 2 a and b). The second group with five weld metals contained larger or smaller regions

with a morphology suggesting a mixed ferritic-austenitic solidification (Figure 2 c and d). It was noted that the ratio between the Cr- and Ni-equivalents from the WRC-92 diagram could be used to predict the solidification mode (Table 4) if weld metals with a Cr content below 22% and those with approximately 23%Cr or higher (Table 2) were treated separately. For the lower Cr weld metals the shift took place between $Cr_{eq}/Ni_{eq}=2.14$ and a ratio of 2.18 whereas for the higher Cr level the change occurred between 1.83 and 1.89. All welds were free from significant amounts of nitrides and contained only minor amounts of secondary ferrite.

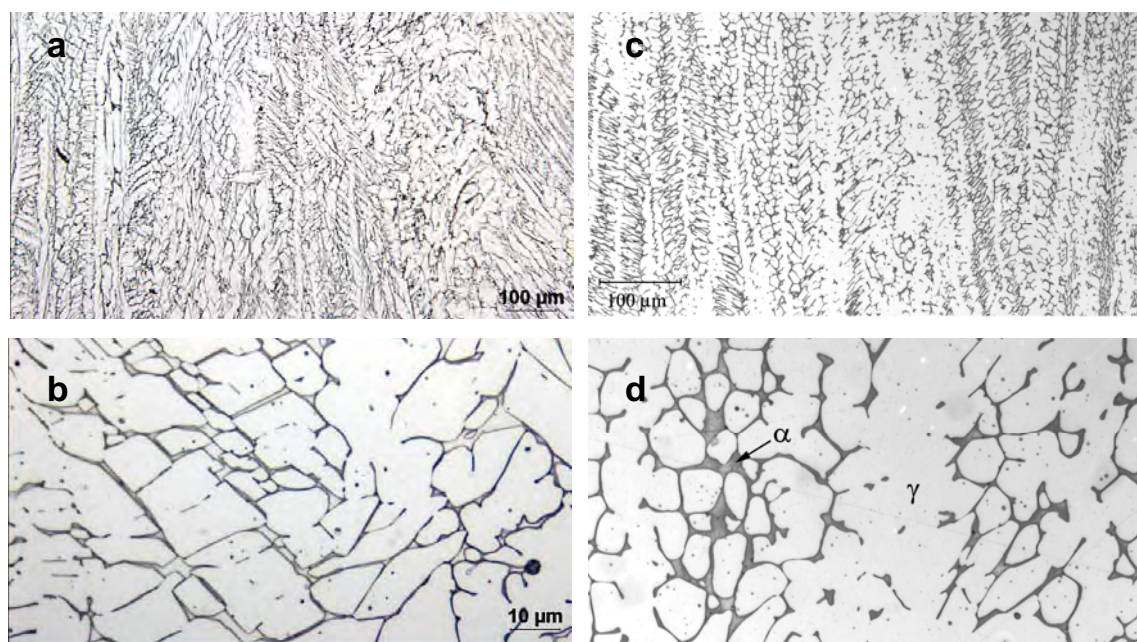


Figure 2. (a and b) Reheated region microstructures of weld metal No. 12 with a typical duplex microstructure throughout although with a low ferrite content of approximately 22 FN. (c and d) A reheated region in weld metal No. 6 having a morphology with ferrite (α) located mainly interdendritically and forming an almost continuous network typical of mixed austenitic-ferritic solidification. The average ferrite content was 16 FN.

Table 4. Predicted and measured ferrite number (Ferrite Number (FN)) and observed solidification modes of experimental lean duplex all-weld metals.

Property	Weld											
	1	2	3	4	5	6	7	8	9	10	11	12
Measured FN, center	22	33	15	36	35	23	31	41	38	38	27	22
Predicted FN*	19	25	16	29	21	23	29	45	50	50	33	26
Cr_{eq}/Ni_{eq} *	1.74	1.89	1.79	2.14	2.01	1.83	1.97	2.28	2.31	2.51	2.33	2.18
Solidification mode*	FA (+F)	F	FA (+F)	FA + F	F (+FA)	FA + F	F	F	F	F	F	F

* According to the WRC-1992 diagram **F = fully ferritic, FA = Ferritic/austenitic

Discussion

Leaving weldability and cost aspects aside it is essential to design a lean duplex consumable in such a way that required mechanical properties and corrosion resistance can be guaranteed.

Corrosion

Corrosion resistance was estimated using the well established $PRE_N = Cr + 3.3Mo + 16N$ formula. The three Mo-free LDSS steels in Table 1 have minimum PRE_N values of 20-24 and

typical values of 25 or less. The consumable should therefore be designed to have typically a higher PRE_N than 25 and a minimum value of 24. Although not reflected in the formula it is known that substituting Mn for Ni will lower corrosion resistance [7]. Ni-rich compositions can therefore be expected to perform better than Mn-rich compositions at similar PRE_N values.

Strength and ductility

The minimum required strength of lean duplex steel grades is in the range 400 MPa to 450 MPa in yield and 600-690 MPa in tensile strength depending on grade and product form according to ASTM/ASME standards. These levels were matched with a significant margin for all weld metals in the present study on MMA weld metals (Table 3) as well as those in a previous study on weld metals deposited with metal cored wires [5]. Elongation was in all cases at 24% or higher which is well above the requirement (EN and AWS) of 20% for standard 2209 type consumables.

Impact toughness and microstructure

Although LDSS are not designed or typically recommended for low temperature applications a reasonable aim is a minimum weld metal impact toughness of 27 J at -40°C . Several factors, many of those interacting, are known to affect impact toughness. This makes it difficult to visualise effects in simple diagrams looking at one factor only. However, pooling data from the present MMA weld metals and the previous study on weld metals produced with metal cored wires [5] and plotting ferrite content against impact toughness (Figure 3) clearly illustrates that solidification mode and the resulting ferrite morphology has to be considered.

Excluding weld metals with a mixed austenitic-ferritic solidification morphology (Figure 3b) decreases scatter, raise average levels both at -20°C and at $+20^{\circ}\text{C}$ and separate the two test series. There is however no clear tendency of increasing toughness with decreasing ferrite content as is normally expected [8].

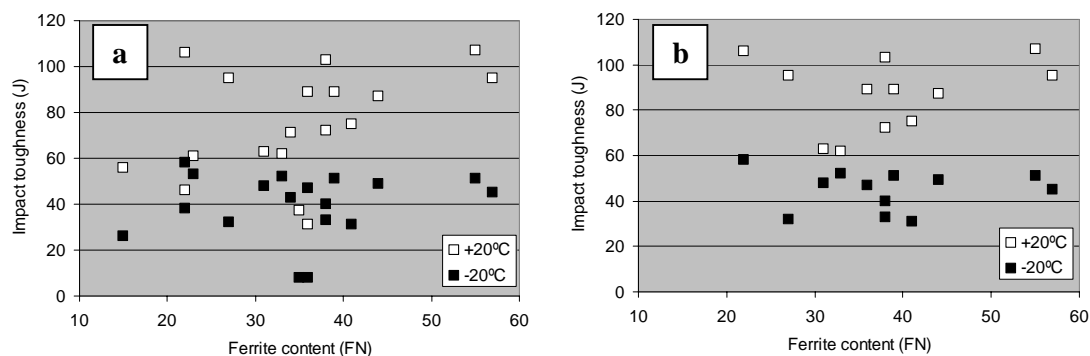


Figure 3. Impact toughness of lean duplex MMA weld metals and MIG weld metals produced with metal-cored wires as a function of weld centre ferrite content. Diagram (a) includes all welds whereas those having a morphology with ferrite located mainly interdendritically and forming an almost continuous network typical of mixed austenitic-ferritic solidification are excluded in diagram (b).

Another factor known to affect toughness is the inclusion content, mainly governed by oxygen content, but the oxygen variation between 0.05% and 0.11% could not clearly be correlated to properties. The same observation was made when simple correlations between individual alloying elements such as Mn and N were sought. However, there was a slight tendency that impact toughness decreased with increasing tensile strength which was generally higher for the high Mn + N alloys (e.g. weld metal 4, 5, 10 and 11 in Table 3). Consequently there was an indirect effect of these elements. Another related effect is illustrated in Figure 4 showing impact toughness at different temperatures as a function of Ni-content. Weld metals with a ferritic-

austenitic solidification were again excluded to avoid confusing results. The low Ni weld metals are those with a higher Mn- and mostly also a higher N-content making it impossible to study the effect of Ni alone. It can be noted though that the temperature dependence becomes much more pronounced with decreasing Ni-content. A too low Ni-content is therefore not recommendable if reliable toughness properties are required at sub-zero temperatures.

Optimum weld metal composition

Considering all the above aspects an optimum weld metal composition should be low in Mn, have a Ni content preferably above about 7% and have N-, Cr- and Mo-contents that assure a fully ferritic solidification and a PRE_N of about minimum 25. A proposed composition of 23-24%Cr, 7-8%Ni, 0-0.3%Mo and 0.12-0.16%N will fulfil all these requirements. It might be appropriate, though, to add a requirement on a minimum ferrite content. If ferrite-forming elements are at their lower limits at the same time as austenite formers are close to their upper bounds it is otherwise possible to produce lower than normally desired ferrite contents.

Conclusions

- Microstructure and properties of lean duplex MMA weld metals were studied for selected combinations of Mn, Ni and N and Cr.
- Two individual factors were found to be critical to produce acceptable impact toughness at room and sub-zero temperatures: 1) A fully ferritic solidification producing a “typical duplex” weld metal microstructure and 2) a sufficient Ni-content.
- It was concluded that a composition of 23-24%Cr, 7-8%Ni, 0-0.3%Mo and 0.12-0.16%N was well suited to fulfil requirements on mechanical properties and corrosion resistance.

References

- [1] “Practical guidelines for the fabrication of duplex stainless steels”, IMO, London, England, 2001
- [2] M. Benson, “Applications utilising the advantageous properties of LDX 2101”, Proc. Stainless Steel World’2005, Maastricht, The Netherlands, Nov. 8-10, 2005, 171-176
- [3] P. Stenvall and M. Holmquist, “Weld properties of Sandvik SAF 2707”, Proc. Duplex’2007, Grado, Italy, June. 18-20, 2007
- [4] C. Charles, “Duplex stainless steels, a review after DSS’07 held in Grado” Proc. Stainless Steel World’2007, Maastricht, The Netherlands, Nov. 6-8, 2007, Paper K05
- [5] L. Karlsson, S. Rigdal, E.-L. Bergquist and H. Arcini, “Effects of alloying elements on properties of duplex stainless steel weld metals”, Proc. Duplex’2007, Grado, Italy, June 18-20, 2007
- [6] B. Sundman, B. Jansson and J.-O. Andersson, CALPHAD, 1985, Vol. 9, pp. 153-190
- [7] R.F.A. Jargelius-Pettersson, “Application of the Pitting Resistance Equivalent to some highly-alloyed austenitic stainless steels”, Corrosion, Vol. 54, No. 2, pp. 807-812, 1996
- [8] S. Pak and L. Karlsson, “Optimizing the properties of duplex stainless weld metals by addition of nitrogen” Scand. Journal of Metallurgy. Vol. 19, No. 1, 1990, pp. 9-13.

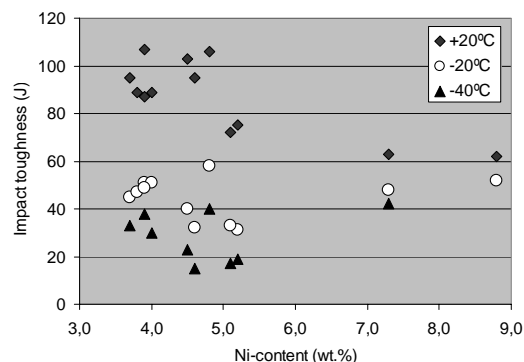


Figure 4. The influence of lean duplex weld metal Ni-content on impact toughness. Only weld metals with a microstructure typical of a fully ferritic solidification are included in the diagram.

MICROSTRUCTURE AND CORROSION PROPERTIES OF STAINLESS STEEL STRIP WELDS

S. Wessman, R. Pettersson

Corrosion & Metals Research Institute (KIMAB), Sweden

Abstract

Strip welding is an efficient method for cladding structures such as pressure vessels in order to provide a corrosion resistant surface. The deposited weld metal thickness is typically 5-10 mm depending on the number of layers employed. This work focuses on welds with compositions around 18Cr 13Ni 3Mo, made with either a single layer, a dual layer or a single layer with alloying additions via the flux. The observed solidification structures show austenitic dendrites with around 5% interdendritic ferrite. Alloying element partitioning agrees with that predicted from equilibrium and Scheil-Gulliver calculations using the Thermo-Calc database. Pitting corrosion in NaCl and uniform corrosion in hydrochloric and sulphuric acids is concentrated in the austenite dendrite centres. This reflects the lower levels of chromium and molybdenum contents at these sites and can be correlated to the calculated Pitting Resistance Equivalent.

Introduction

Electroslag strip cladding (ESW) is an attractive method for rapid deposition of a higher alloyed, usually more expensive, protective surface layer on a less corrosion resistant load bearing bulk material [1]. The method developed from submerged arc welding (SAW) and involves feeding of a strip material with flux added as powder. The difference is that ESW is an arcless method which uses ohmic heating to melt strip, flux and parent material. Advantages compared to SAW include a 60-80% increase in deposition rate, less dilution from base material and 50-100% increased weld speed, giving a higher area cover and less flux consumption [2]. The principles of electroslag strip cladding are shown in Figure 1. Recent developments of fluxes [3] introduce the possibility to reduce the amount of strip materials to a standard repertoire and instead use different alloyed fluxes to meet customer demands regarding alloying grade for certain applications.

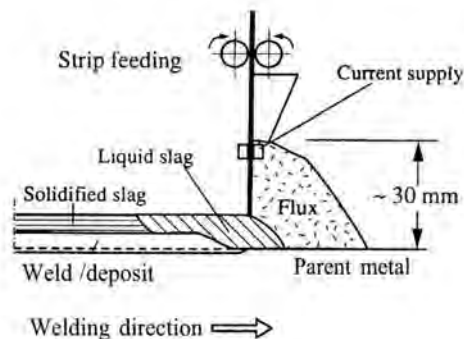


Figure 1. Principles of electroslag strip cladding (ESW) [1]

Experimental

Three strip welds of approximately 1 m length and 65 mm width were made on a C-Mn steel with a maximum C-content of 0.20%. The welding parameters were DC+ with 1200 A and 24 V, travel speed 15 cm/min and stick-out 25-30 mm. IM1 and IM3 were single layer welds with a maximum height of about 6 and 8 mm respectively. IM2 was a two layer weld made using a lower alloyed strip (309LMo) for the 1st pass and a higher alloyed (317L) for the 2nd pass, this resulted in a maximum weld height of about 11mm. A standard fluoride basic flux for electro slag strip cladding with austenitic strips was used for IM1 and IM2. For IM3 a modified flux with additions of Ni, FeCr and FeMo was used. Chemical composition of the strip materials is given in Table 1 and for and for welds in Table 2. The analyses were made by optical emission spectroscopy (OES) on top surface with a LECO technique for the nitrogen content.

Table 1. Chemical composition of strip material, wt-% ,Fe balance

	C	Si	Mn	P	S	Cr	Ni	Mo	Cu	N
309LMo	0.010	0.29	1.77	0.007	<0.001	20.4	14.1	2.9	0.09	0.037
316L	0.017	0.64	1.86	0.030	0.004	17.2	12.8	2.6	0.44	0.027
317L	0.017	0.38	1.54	0.014	0.012	18.9	13.5	3.4	0.12	0.046

Table 2. Chemical composition of welds, wt-% ,Fe balance

	Strip	Flux	C	Si	Mn	P	S	Cr	Ni	Mo	Cu	N
IM1	317L	Standard	0.019	0.56	1.17	0.022	0.007	17.39	12.59	3.13	0.12	0.038
IM2 (1)	309LMo	Standard	<i>1st weld pass not analysed!</i>									
IM2 (2)	317L	Standard	0.014	0.56	1.19	0.022	0.006	18.58	13.44	3.26	0.12	0.042
IM3	316L	Modified	0.021	0.20	0.94	0.038	0.003	18.31	13.20	3.28	0.43	0.032

Uniform corrosion was assessed by weight loss of all-weld specimens after exposure to 5% HCl or 30% H₂SO₄ at 50°C for one week. Before testing specimens were wet ground to 600 mesh. After immersion in the test solution, the surface was activated by touching with a piece of zinc so that hydrogen was evolved on the specimen and the passive film removed [4]. CPT-testing was done according to ASTM G150 in 1M NaCl solution and are given as solution temperatures. The specimens were wet ground to 600 mesh at least 18 hours before testing. In order to identify the sites for pit initiation in the welds, immersion testing was done in solution of 15 g FeCl₃, 15 g AlCl₃, 100 ml glycerol and 100 ml ethanol [5] at 40°C. Polished specimens were immersed for about 20-30s and then evaluated using LOM and SEM. This method usually gives selective attack, which reveals which phase or area of the microstructure has the lowest resistance to pitting corrosion.

Microstructure

The microstructure in all cases comprised a predominantly austenitic structure with a small amount of an interdendritic phase, Figure 2. The ferrite numbers were in the range 6-8 and agreed reasonably with the WRC-92 diagram [6] which predicted ferrite numbers in the range 4-7. Imaging in SEM showed that the interdendritic phase was predominantly ferrite, but there was also a small amount of sigma phase present in all three welds; this was confirmed using EBSD.

Equilibrium and Scheil calculations using Thermo-Calc [7,8] agreed well with the observed microstructures, and predicted ferrite and austenite to form from the melt and austenite to dominate on continued cooling. At lower temperatures small amounts of sigma and chi phases are predicted stable as are small amounts of carbides and nitrides. An example is given in Figure 3 for weld IM3 but there were no significant differences between the three welds.

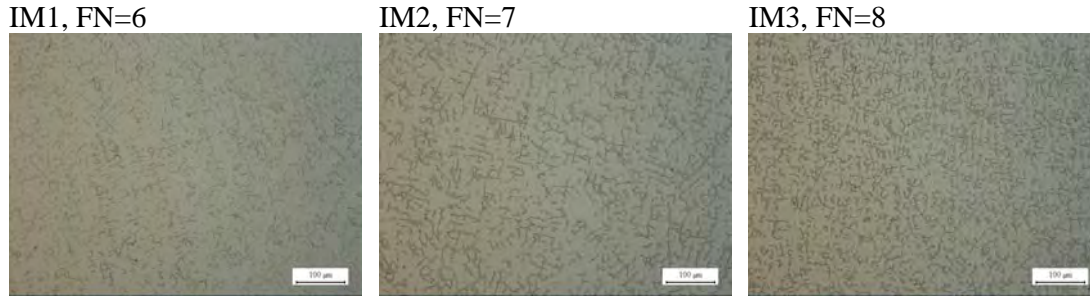


Figure 2. Microstructure and ferrite numbers, measured with a Fischer MP30 Feritscope, after milling 2mm from the outer surface. Etchant 100 ml H₂O, 100 ml HCl, 20 ml HNO₃.

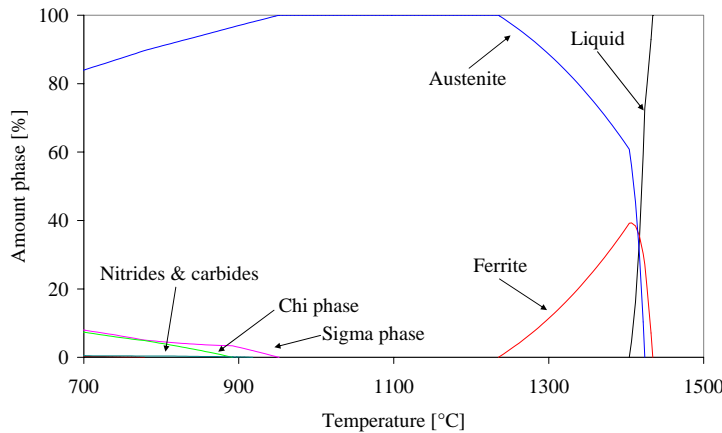


Figure 3. Thermo-Calc equilibrium calculation showing stable phases [%] vs. temperature [°C] for weld IM3

Analyses of weld chemical composition were made at start, centre and end position of each weld in a round robin manner at three laboratories. The observed deviations were within the margin of error for the analysis methods and confirmed experience from producers that the process is very stable. The variation in weld composition as a function of depth was analysed using EDS at a low magnification in SEM. The vertical field height was approximately 0.1 mm and analysis was performed on an area of 500x50 µm in the centre of each field. The results in Figure 4 show that there has been excellent mixing over the entire weld depth, with only slight deviations very close to the fusion line. For the two-layer weld IM2 there was a slight shift in molybdenum concentration at 5 mm depth which corresponds to the transition between 317L strip with 3.4% Mo to 309LMO with 2.9%.

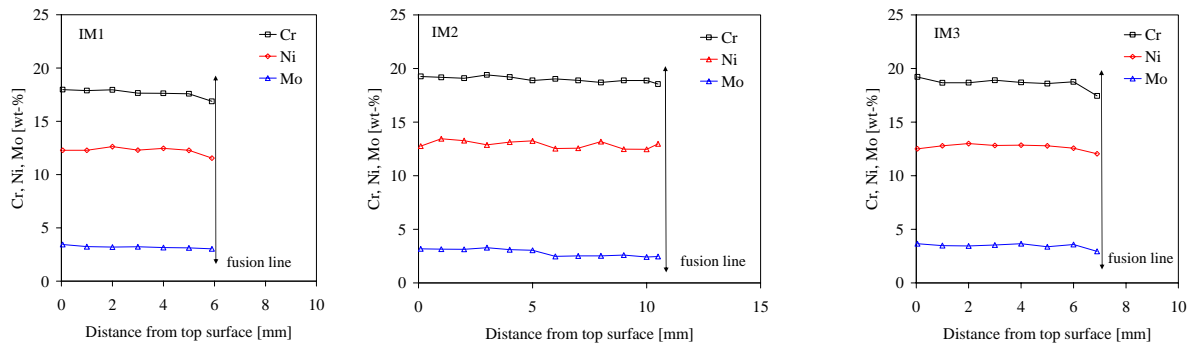


Figure 4. Depth profile for Cr, Ni and Mo [wt-%] vs. distance from top surface [mm]

Microsegregation was quantified by making an array of EDS point analyses at a magnification of 1000x on specimens which had been milled down to 2mm below the original weld surface. A total of 500 analysis points were made for each weld and the data is plotted on normal probability axes in Figure 5. In such a plot a higher standard deviation is manifested as a higher slope. Bimodal distributions were obtained because of the two phase structure. The upturn in chromium and downturn in nickel is due to the presence of ferrite, and it can be seen that this occurs at similar area fractions for all three welds, in agreement with the ferrite number measurements reported above.

The absolute values of the Cr and Ni contents were highest for IM2 and lowest for IM1, but the curves for all three welds were parallel, indicating a similar degree of segregation. The maximum compositional variation within the austenite phase was approximately 2% Cr and 3% Ni. Weld IM3 had the highest molybdenum content and also showed marginally higher degree of segregation. This was primarily manifested as a higher molybdenum content in the ferrite. The manganese and silicon distributions were very similar for welds IM1 and IM2, while for weld IM3 the absolute values were lower and the degree of segregation slightly higher.

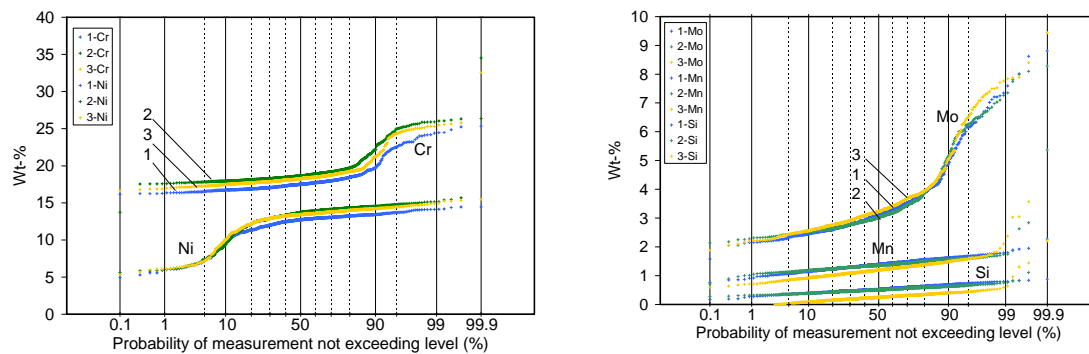


Figure 5. Probability plots of EDS measurements on five fields of 10 x 10 points with a point spacing of approximately 5 μ m. The highest Cr and Mo levels, and lowest Ni levels, are from the ferrite phase.

Corrosion properties

The results from the uniform corrosion testing in acids are calculated in mm/year and given in Figure 6. In both solutions the weight loss was highest for IM1 and lowest for IM3. There are two factors which may contribute to this: firstly that the weight loss specimen of IM2 also included the lower alloyed 309L weld metal from the first pass, secondly that the slightly higher Cu content of IM3 may make a positive contribution to uniform corrosion resistance.

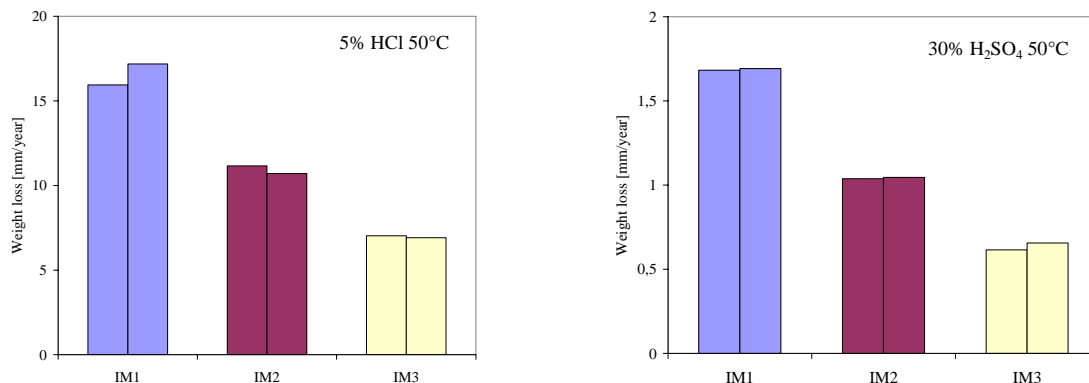


Figure 6. Results from weight loss testing in 5% HCl (left) and 30% H₂SO₄ (right) at 50°C [mm/year].

The results from CPT testing in 1M NaCl are summarised in Figure 7. Reproducibility was good and no difference in corrosion resistance was found between the positions start (1), centre (2) and end (3). Weld IM1 had a CPT of about 20°C, while that for IM2 and IM3 was about 25°C. These figures are lower than the values of 29°C and 41°C measured for the unwelded 316L and 317L strip material [9] but are reasonable for welds. The difference between IM1 and IM2 or IM3 was significant at the 5% level, but there was no significant difference between IM2 and IM3. The CPT values correlate well to the PRE (Pitting Resistance Equivalent), which was calculated as $PRE=Cr+3.3Mo+16N$ [10]. This yielded 28 for IM1 and 30 for IM2 and IM3.

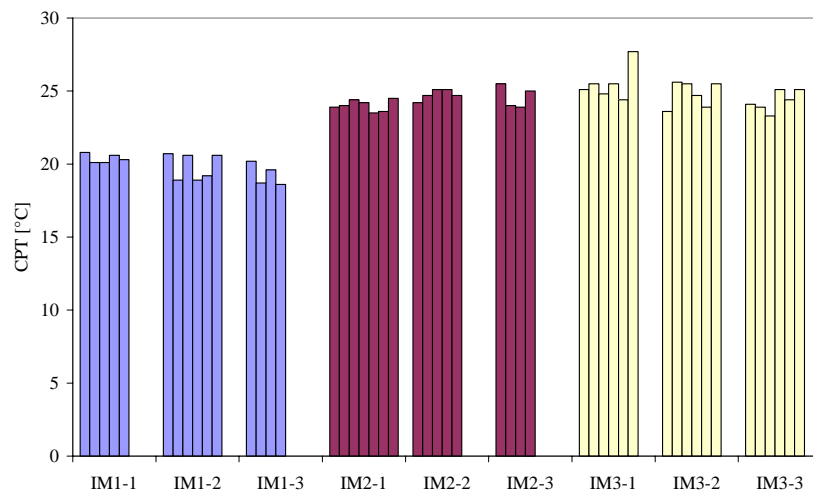


Figure 7. Results from CPT-testing in 1M NaCl [°C] for welds IM1-3, figures 1-3 denotes start (1), centre (2) and end (3).

The immersion testing $FeCl_3+AlCl_3$ +glycerol+ethanol gave clusters of small pits in the centres of austenite dendrites, Figure 8. This distribution shows that the compositional gradients within the austenite are sufficiently large to affect corrosion resistance. The pit location agrees with PRE-calculations from the Scheil-Gulliver calculations, which indicate the first formed austenite to be the least corrosion resistant component, Figure 9.

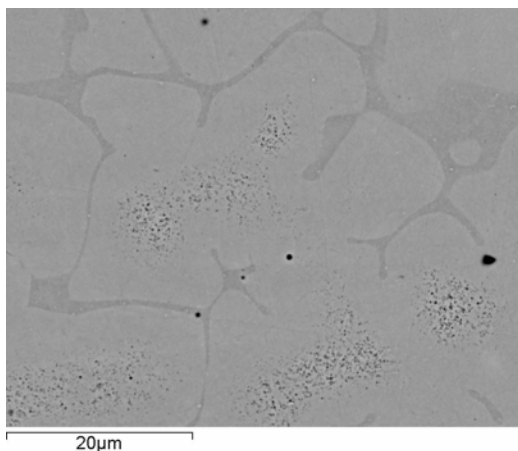


Figure 8. SEM-BS images of pits in IM2 after immersion testing, showing clusters of pits in the austenite dendrite centres and no pitting adjacent to the ferrite phase.

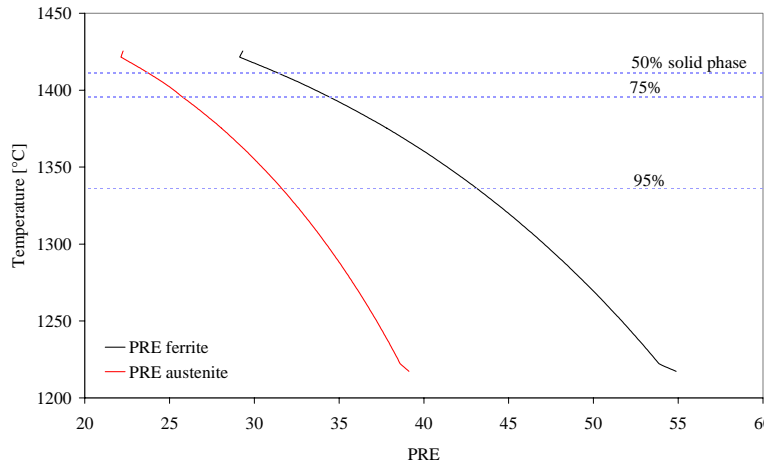


Figure 9. Scheil-Gulliver PRE estimation for IM2, displaying the austenite (lower PRE) as the less pitting corrosion resistant phase.

Summary and conclusions

The aim of this work was to investigate microstructure and corrosion properties of electroslag strip cladding (ESW) weld metal of 316 type. The welds were a single layer weld with 317L strip, a standard two-layer weld with 309LMo+317L strip and a single-layer weld with 316L strip in combination with an alloyed flux.

Results show no major differences in solidification mode, microstructure, segregation or interdendritic phases in the three welds. Ferrite contents were in the region 6-8 FN and there was a small amount of sigma phase present in the as-welded condition. The CPT and uniform corrosion resistance in H_2SO_4 and HCl at 50°C was lowest for the conventional single-layer weld with 317L strip. The dual-layer weld with 309LMo+317L strip and the single-layer weld with 316L strip plus alloyed flux exhibited no significant difference in CPT.

Acknowledgements

This project was carried out within the member programme “Institutet för Metallforskning” at KIMAB with the support of ESAB AB and AB Sandvik Materials Technology.

References

- [1] S. Pak, S. Rigdal, L. Karlsson A.-C. Gustavsson: Svetsaren, No. 3, 1996, pp. 28-33
- [2] R. Paschold: Svetsaren, No. 2-3, 2001, pp. 62-67
- [3] L. Karlsson, S. Pak, S. Rigdal: Proc. Stainless Steel World 99, pp. 587-593, The Hague, The Netherlands, 16-18 November 1999, KCI Publishing BV
- [4] U. H. Kivisäkk: Corrosion, Vol. 61, no. 6, June 2005, pp. 602-608
- [5] G. Bianchi, A. Cerquetti, F. Mazza, S. Torchio: Corr. Science, Vol. 10, 1970, pp. 19-27
- [6] The Avesta Welding Manual, 2004
- [7] B. Sundman, B. Jansson, J. O. Andersson: Calphad, Vol. 9, April-June 1985, pp. 153-190
- [8] Thermo-Calc Version Q running on PC/Windows NT and databases TCS Steel v.3
- [9] S. Wessman, R. Pettersson, L. Karlsson, S. Rigdal, P. Stenvall, Corrosion and Metals Research Institutet report KIMAB-2007-534
- [10] J. E. Truman: Proc. U.K. Corrosion -87, pp. 111-129, Brighton, UK, October 26-28, 1987, Institution of Corrosion Science & Technology, Birmingham, U.K.